Regional characteristics of fine aerosol mass increase elucidated from long-term observations and KORUS-AQ campaign at a Northeast Asian background site

Lim, Saehee

2022-09-30

Lim , S , Lee , M , Laj , P , Kim , S W , Ahn , K H , Gil , J , Shang , X , Zanatta , M & Kang , K S 2022 , ' Regional characteristics of fine aerosol mass increase elucidated from long-term observations and KORUS-AQ campaign at a Northeast Asian background site ' , Elementa , vol. 10 , no. 1 , 00020 . https://doi.org/10.1525/elementa.2022.00020

http://hdl.handle.net/10138/355415
https://doi.org/10.1525/elementa.2022.00020

ELEMENTA
Science of the Anthropocene

Lim, S, et al. 2022. Regional characteristics of fine aerosol mass increase elucidated from long-term observations and KORUS-AQ campaign at a Northeast Asian background site. *Elem Sci Anth*, 10: 1. DOI: https://doi.org/10.1525/elementa.2022.00020

RESEARCH ARTICLE

Regional characteristics of fine aerosol mass increase elucidated from long-term observations and KORUS-AQ campaign at a Northeast Asian background site

Saehee Lim[1,2], Meehye Lee[1,*], Paolo Laj[3,4,5], Sang-Woo Kim[6], Kang-Ho Ahn[7], Junsu Gil[1], Xiaona Shang[1,8], Marco Zanatta[9], and Kyeong-Sik Kang[10]

Northeast Asia has suffered from severe $PM_{2.5}$ pollution and the exact mechanisms have yet to be fully understood. Here, we investigated the transformation processes of submicron aerosols using a 4-year data set obtained at Jeju, a Northeast Asian background site. The diurnal-cycle constrained empirical orthogonal function analysis of nanoparticle size–number distribution distinguished 2 modes: burst of nucleation–Aitken particles and increase in accumulation mode particles, representing "new particle formation and growth" and "$PM_{2.5}$ mass increase," respectively. In these events, aerosol and meteorological characteristics changed progressively over several days, revealing that the $PM_{2.5}$ mass increase is an episodic event occurring on a regional scale. The increase in $PM_{2.5}$ mass was accompanied by an increase in aerosol liquid water content, which correlated well with SO_4^{-2} and NO_3, and a decrease in incoming solar radiation (-14.1 Wm^{-2} day^{-1}) constituting a positive feedback. The "transport/haze" episode of KOREA–U.S. Air Quality campaign corresponds to "$PM_{2.5}$ mass increase," during which the vertical evolution of particles demonstrates that nanoparticles $\geq$3.5 nm were entrained into the shallow boundary layer upon vertical mixing and converted to accumulation-mode particles $\geq$0.3 μm at relative humidity (RH) exceeding the deliquescence RH of secondary inorganic aerosol (SIA). Coincidently, at ground, the coating thickness of refractory black carbon (rBC) (48 $\pm$ 39 nm) and SIA concentration increased. Furthermore, the diameter of rBC (180–220 nm)-containing particle in core–shell configuration linearly increased with $PM_{2.5}$ mass, reaching 300–400 nm at $PM_{2.5} \geq 40$ μg m^{-3}. This observational evidence suggests that the thick coating of rBCs resulted from the active conversion of condensable gases into the particulate phase on the rBC surface, thereby increasing the mass of the accumulation-mode aerosol. Consequently, this result complies with the strategy to reduce primary emissions of gaseous precursors for SIA and particulates such as rBC as a way to effectively mitigate haze pollution as well as climate change in Northeast Asia.

Keywords: Aerosol number concentration, $PM_{2.5}$ mass increase, Secondary inorganic aerosol, Boundary layer, Refractory black carbon, KORUS-AQ

1. Introduction

Urban areas in Northeast Asia have experienced heavy air pollution over the past few decades. Severe and persistent haze with high levels of $PM_{2.5}$ (particulate matter with aerodynamic diameter smaller than 2.5 mm) has been of major public concern due to its potential adverse effects on human health, such as cardiovascular and respiratory disease and lung cancer, which leads to increased

[1] Department of Earth and Environmental Sciences, Korea University, Seoul, South Korea
[2] Department of Environmental Engineering, Chungnam National University, Daejeon, South Korea
[3] Institute for Atmospheric and Earth System Research, Faculty of Science, University of Helsinki, Helsinki, Finland
[4] University of Grenoble-Alpes, CNRS, IRD, Grenoble INP, Institute for Geosciences and Environmental Research (IGE), Grenoble, France
[5] Department of Physics, University of Helsinki, Helsinki, Finland
[6] School of Earth and Environmental Sciences, Seoul National University, Seoul, South Korea
[7] Department of Mechanical Engineering, Hanyang University, Ansan-si, Gyeonggi-do, South Korea
[8] School of Chemical and Environmental Engineering, Shanghai Institute of Technology, Shanghai, China
[9] Alfred Wegener Institute (AWI), Helmholtz Center for Polar and Marine Research, Bremerhaven, Germany
[10] Jeju Air Quality Research Center, National Institute of Environmental Research, Jeju, South Korea

* Corresponding author:
Email: meehye@korea.ac.kr

risk of mortality (Atkinson et al., 2015; Lelieveld et al., 2015; Apte et al., 2018; Burnett et al., 2018). In Seoul, the capital of South Korea, the annual $PM_{2.5}$ concentration has remained as high as 20–30 μg m^{-3} over the past 10 years (Yeo et al., 2019), easily exceeding the national (15 μg m^{-3}) and World Health Organization (WHO) (10 μg m^{-3}) annual air quality standard. High-concentration $PM_{2.5}$ events tend to occur frequently in the cold months from November to March (Lim et al., 2012; Lim et al., 2014), when the daily average $PM_{2.5}$ concentrations often exceed the national air quality standard (35 μg m^{-3}). Consistently, in China, 56% of regional pollution events occurred during the cold months in 2014–2017 (Li et al., 2020). The chemical composition of the cold-month high $PM_{2.5}$ is dominated by secondary inorganic aerosols (SIAs), namely SO_4^{-2}, NO_3^-, and NH_4^+ (e.g., Huang et al., 2014; Liu et al., 2018). In comparison, organic carbonaceous aerosol accounts for a large proportion in fine aerosol mass during warm months (e.g., Kim et al., 2018). Meanwhile, black carbon (BC) that is directly emitted to the atmosphere from combustions of biomass and fossil fuel, a strong climate forcer (Bond et al., 2013; Boucher et al., 2013), has been recently known that its small, insoluble, and inert nature facilitate its long-range transport across China during haze pollution events (Wang et al., 2016; Zheng et al., 2019). Co-emitted with various gaseous precursors (e.g., NO_x and SO_2) and particulates, BC undergoes physical evolution in size and mixing state upon transportation through the formation of coatings by non-BC materials after being emitted (Lim et al., 2018; Zanatta et al., 2018; Liu et al., 2019). The occurrence of high-concentration $PM_{2.5}$ events has become a regional characteristic of the Northeast Asia (Liu et al., 2018; Fan et al., 2020).

Long-term regulatory actions to control emissions have been implemented in South Korea as well as China. However, severe $PM_{2.5}$ events have been frequently encountered over the last few years in Seoul (Park et al., 2021). Current knowledge is insufficient to explain the complex processes that generate unexpectedly high $PM_{2.5}$ masses (e.g., An et al., 2019). Most of all, aerosol formation mechanisms and the interplay of physicochemical transformation mechanisms with meteorological conditions that are vital for the effective mitigation of haze pollution, have yet to be fully identified.

Theoretically, new particle formation (NPF) and subsequent growth occur via the gas-to-particle conversion of gaseous precursors, such as SO_2, NO_x, VOCs, and NH_3. This process, known as NPF, is primarily dependent on 2 parameters: (1) source strength of condensable gases and (2) pre-existing particles that act as a condensation sink (CS) (Kerminen et al., 2018). It was also found that a minimum in CS correlates with a maximum frequency of nucleation on a regional scale of Europe (Elser et al., 2016). However, in polluted cities of China with high levels of both precursors and CS, NPF occurs frequently, showing distinct features from pristine environments (Kulmala et al., 2017; Chu et al., 2019). For example, nanoparticles undergo rapid and continuous growth in size from smaller than 10 nm to larger than 100 nm in 1 day (Wiedensohler et al., 2009) or from smaller than 50 nm to larger than 200 nm in a couple of days (Guo et al., 2014), even during heavy pollution episodes. In comparison, the entire processes from nanoparticle formation to increase in fine aerosol mass have rarely been observed in ambient atmosphere including Seoul or background sites in South Korea (e.g., Kim et al., 2013) and may not be explained in the same manner throughout the Asian continent. Therefore, the conditions and mechanisms responsible for the rapid increase in $PM_{2.5}$ mass are still poorly understood.

Recently, meteorological conditions are thought to be closely related to persistent $PM_{2.5}$ haze pollution over China on a regional scale (Wang et al., 2014a; Wang et al., 2014b; Zhang et al., 2018; Wang et al., 2019). Strong correlations of daily $PM_{2.5}$ concentrations with several meteorological variables (local or climate variables) have been found and unambiguous spatial patterns indicate the importance of synoptic meteorology affecting haze developments (Cai et al., 2017; Leung et al., 2018). Among these, the dynamic evolution of planetary boundary layer (PBL) has drawn much attention due to its direct effects on $PM_{2.5}$ concentrations such as stable atmospheric stratification accumulating local emissions, positive feedback between boundary layer stability and pollution intensity, and downward transport of pollutants from the free atmosphere through PBL processes (e.g., Zhong et al., 2018; Li et al., 2020; Quan et al., 2020). For NPF, the combined effect of boundary layer dynamics and atmospheric chemistry on aerosol composition was emphasized (Song et al., 2010; Hao et al., 2018). As is commonly observed during several haze events, high relative humidity (RH) is believed to facilitate the hygroscopic growth of SIAs, thereby increasing $PM_{2.5}$ concentrations (Zhang et al., 2015; Wang et al., 2019). Recent studies have highlighted the role of aerosol liquid water content (ALWC) in the rapid formation of SIAs in Northeast Asia (Liu et al., 2017; Wu et al., 2018). ALWC is known to depend on RH and, mass and chemical composition of aerosols (Pilinis et al., 1989). At high RH, ALWC will increase uptake coefficients of N_2O_5, thereby enhancing the formation of particulate nitrate (Bertram and Thornton, 2009; Bertram et al., 2009). Recently, an isotope-based field study that shows wintertime NO_3^- concentration formed via the N_2O_5 pathway increased with ALWC in Seoul (Lim et al., 2022). It has already been suggested that ALWC promotes the aqueous conversion of SO_2 to SO_4^{-2}. However, a comprehensive and systematic understanding of particle formation/transformation and haze developments is hindered by the complexity of local to large-scale meteorology, local emissions versus transboundary transport of pollutants, and particle (trans)formation mechanisms. Therefore, long-term observations in the background region are essential to better understand the phenomena on a regional scale.

In this study, we thoroughly examined the size-separated aerosol number distributions in relation to the mass of $PM_{2.5}$ and its chemical composition, gaseous precursors, and meteorological characteristics observed in the East Asia outflow region for multiple years. Based on the results, we aimed to elucidate general characteristics of mass increase in fine aerosol at a regional site in Northeast Asia.

2. Methods

2.1. Long-term measurements

A suite of aerosol instruments was deployed to measure aerosol number concentrations, $PM_{2.5}$ mass concentrations and its chemical constituents, the mixing ratios of reactive gases, and meteorological parameters at the Jeju Air Quality Monitoring Research Center (33.21°N, 126.23°E, 600 m asl; hereinafter referred to "Aewol") in Jeju Island, South Korea (Figure S1), from January 2013 to December 2016. This station has been served as the national background air pollution monitoring station without evidently significant local pollution sources.

The number concentrations of size-separated particles at diameter (Dp) ranging from 10.4 to 469.8 nm were measured every 30 min by the scanning mobility particle sizer (SMPS, model 3034, TSI, USA), and $PM_{2.5}$ mass concentrations were measured every hour by the beta attenuation mass monitor (BAM1020, MetOne Instrument Inc., OR, USA). For $PM_{2.5}$ chemical composition, water-soluble ions and organic and elemental carbon (OC and EC) were determined. Water-soluble ions were measured every hour by a Monitor for Aerosols & Gases in Ambient Air (MARGA, Metrohm, Switzerland). OC and EC concentrations were simultaneously determined with the thermal/optical transmittance method (NIOSH 870 protocol) by a Sunset Lab OCEC Analyzer (Sunset Laboratory Inc., OR, USA). Reactive gases including SO_2, NO_2, NH_3, and O_3 were continuously monitored, and their nominal detection limits were 0.1 ppbv, 0.1 ppbv, 0.1 ppbv, and 2 ppbv, respectively (An et al., 2015). These instruments were calibrated and checked up on a weekly, monthly, or annual basis according to the information provided by the manufacturer and guidelines established by the Ministry of Environment and National Institute of Environmental Research (National Institute of Environmental Research, 2021). Details about measurement methods can be found elsewhere (e.g., Shin et al., 2016; Park et al., 2018).

Meteorological variables including temperature, RH, wind speed and direction, SO_2, and cloud properties were measured at Gosan Climate Observatory (GCO, 33.17°N, 126.10°E) in Jeju Island by Korean Meteorological Administration (KMA, https://data.kma.go.kr/cmmn/main.do). In addition, a set of cloud fraction (low- and mid-level clouds; 1–10 in fraction) and the base height of cloud were measured with a ceilometer (CL31, Vaisala), which were incorporated into the measurements at Aewol. All measurements were assimilated into 1-h averages.

2.2. 2016 KORUS-AQ campaign

The Korea–U.S. Air Quality (KORUS-AQ) campaign provided a unique opportunity to observe distinctive events from May to June 2016. Along with measurements at Aewol, the physical properties of refractory BC, including number and mass concentrations, size distributions, and mixing state (coating thickness), were determined at GCO using the Single Particle Soot Photometer (SP2, Droplet Measurement Technology, Boulder, CO, USA) (Stephens et al., 2003; Schwarz et al., 2006; Moteki and Kondo, 2010).

SP2 utilizes a laser-induced incandescence technique to quantify the mass of a single refractory BC (Petzold et al., 2013). For individual detection of incandescence and scattering signals, the SP2 is equipped with 2 photomultiplier tubes and 2 avalanche photodiodes, each yielding high- and low-gain values. The incandescence detector was calibrated using well-characterized fullerene soot particles (Alfa Aesar; #FS12S011), and the scattering detector was calibrated with a spherical polystyrene latex size standard (PSL, refractive index (RI) = 1.59; Thermo Fisher Scientific, Waltham, MA, USA) (Baumgardner et al., 2012; Laborde et al., 2012). The detection range of a single-particle mass is 0.33–128 fg, corresponding to rBC mass equivalent diameters (D_{rBC} = 70–514 nm), assuming a void-free material density of 1.8 g cm^{-3} (Bond et al., 2006). To correct for the rBC mass outside the lower detection limit, the rBC mass size distribution was fitted with a lognormal function, and a correction was achieved by adding 10% of the total uncorrected rBC mass on average. An rBC mass larger than the upper detection limit was treated as the largest mass detectable, that is, 128 fg.

Basically, adopting the leading-edge-only approach (LEO approach; Gao et al., 2007; Laborde et al., 2012), the optical diameter of the rBC-containing particle, D_{shell}, was inferred from the leading-edge scattering signal using Mie theory with RI of $1.5 - 0i$ and $2.26 - 1.26i$ for the rBC coating material and rBC core, respectively, at an SP2 operating wavelength of 1064 nm. These RI values have been suggested in previous studies: $2.26 - 1.26i$ for bare or freshly emitted ambient rBC particles (Moteki and Kondo, 2010; Taylor et al., 2015) and $1.5 - 0i$ for inorganic salts and secondary organic aerosol (Toon et al., 1976; Schnaiter et al., 2003) have been used for similar LEO approaches (e.g., Schwarz et al., 2008; Laborde et al., 2013). The coating thickness of individual rBC particles was determined as $(D_{shell} - D_{rBC})/2$. In this SP2, D_{shell} was detectable in the range of 170–500 nm. The proper range of D_{rBC} for LEO approach varies mainly depending on the instrumental setup of the SP2. To ensure the quality of LEO results, lower and upper bounds of D_{rBC} are selected by examining detectable optical diameter of small rBC core (here, $\geq$95%) and a saturation point of the low gain scattering detector (Taylor et al., 2015), respectively. In the present study, D_{rBC} for LEO approach was restricted to the rBC core with a D_{rBC} of 180–220 nm (Laborde et al., 2013; Zanatta et al., 2018). Coating was defined as a thickness larger than 10 nm, considering the systematic uncertainty involved in its estimation (Laborde et al., 2013). Measurements of rBC particle concentration, size distribution, and mixing state of rBC particles were averaged hourly, merged with the $PM_{2.5}$ chemical measurement data set, and used for subsequent discussion.

In addition, vertical profiles (up to 2,500 m) of size-segregated aerosol number concentrations and meteorological parameters were obtained by balloon measurements in Ansan as a satellite city of Seoul (33.17°N, 126.10°E, 70 m asl) (Figure S1). Balloon was launched at 11:26–11:45 on 20 May, and at 8:55–09:05 and 16:05–16:13 on 25 May (local time). Aerosol number concentrations were measured by lab-made instruments at Hanyang University

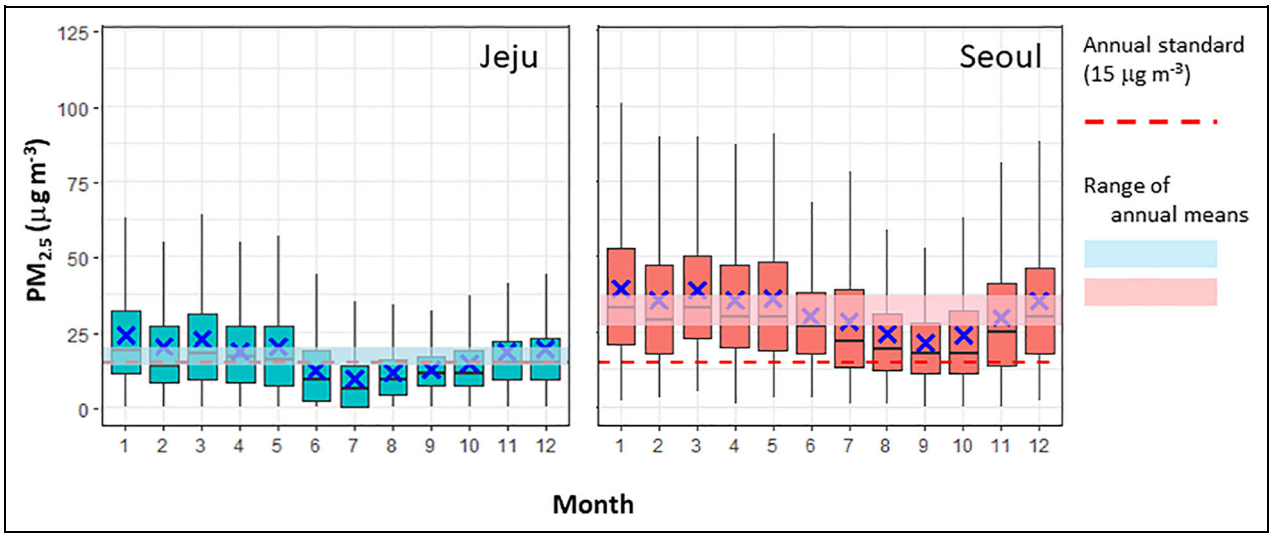

Figure 1. Comparison of monthly variations in $PM_{2.5}$ mass concentration observed in Jeju (Aewol, left) and in Seoul (Bulgwang, right) during 2013–2016. The boxes indicate the inner quartiles, along with the median and the 5th–95th percentiles. The blue and pink shades represent the range of annual mean $PM_{2.5}$ concentrations from 2013 to 2016. The dotted line indicates the national air quality standard of annual mean $PM_{2.5}$ (15 μg m^{-3}).

including condensation particle counter (CPC) for particles larger than 3 nm and 2 optical particle counters (OPCs) for accumulation-mode particles ($particle_{0.3–0.5\ \mu m}$ and $particle_{0.5–1.0\ \mu m}$) (Lee et al., 2014). The number concentration of nanoparticles ($particle_{0.3\ nm–0.5\ \mu m}$) was reported as difference between CPC and OPC. For CPC and OPCs, sampling rate and counting resolution was 0.125 L min^{-1} and 1 s, respectively. The results of vertical measurements using these instruments can be found elsewhere (Querol et al., 2017; Querol et al., 2018). The vertical profiles of meteorological variables and aerosol number concentrations were analyzed along with the physical properties of refractory BC (Section 2.2). To aid in data interpretation, the ALWC was calculated in "forward mode" using the ISORROPIA-II thermodynamic model (Fountoukis and Nenes, 2007).

3. Results and discussion

3.1. Long-term measurements in Jeju background site

The $PM_{2.5}$ concentration of Aewol was much lower as a level of background site than that of Seoul (**Figure 1**). In Seoul, the annual mean $PM_{2.5}$ concentration ranged from 27.3 μg m^{-3} to 38.3 μg m^{-3} during 2013–2016, exceeding the national annual air quality standard (15 μg m^{-3}) every year. For the same period, the annual $PM_{2.5}$ concentration was 13.9–19.7 μg m^{-3} at Aewol. The daily mean $PM_{2.5}$ concentration violated the air quality standard (35 μg m^{-3}) by 33% of the entire period in Seoul. It is also worth noting that 9% of the entire period exceeded the standard at the background site, Aewol. Despite the difference in $PM_{2.5}$ level, the seasonal variation was similar at the 2 sites with high levels in the cold months, demonstrating that the enhancement of wintertime $PM_{2.5}$ is a significant regional issue over the East Asia (Liu et al., 2018; Fan et al., 2020; Li et al., 2020).

3.2. Detecting the 2 modes of particle number distributions

Continuous measurements of size-separated particle number concentrations, spanning 4 years from 2013 to 2016, were analyzed using an empirical orthogonal function (EOF) method, in which the loading vector was constrained to be periodic with a 24-h period (e.g., Kim et al., 2014). As a result, the first and second mode accounted for a significant fraction of 55% and 9%, respectively, while each of the other modes explained less than 4% of the total variance. The first and second modes, which captured the largest variability, contrasted sharply in the diurnal variations in particle number and size (**Figure 2**). The difference between the 2 modes is explicitly demonstrated when comparing the average number–size distributions of ambient particles for the top 10% days with the highest principal component (PC) scores for each mode (Figure S2a). Thereinafter, these cases were considered to be representative of the 2 modes and referred to as "EOF1" and "EOF2," respectively. Out of the 4-year measurement period, each 143 days were tagged as EOF1 and EOF2, respectively. While EOF1 frequently occurred in May and October, the monthly frequency of EOF2 was high in March and June (Figure S2b). In EOF2, the mode of number, surface area, and volume was larger in size, compared to EOF1 (Figure S3). Using these particle number distributions, CS was calculated for the entire range of diameters from 10 nm to 470 nm (Text S1) (Kulmala and Kerminen, 2008). In the following section, particle number–size distributions and levels of CS and gaseous precursors will be compared between EOF1 and EOF2.

In EOF1, the variation of the number concentration corresponds to what used to be observed during the NPF and growth event. The nucleation- and Aitken-mode particles dominated number concentrations with the maximum number concentration greater than 10^4 cm^{-3} at approximately 10–30 nm around noon (**Figure 2c**). They

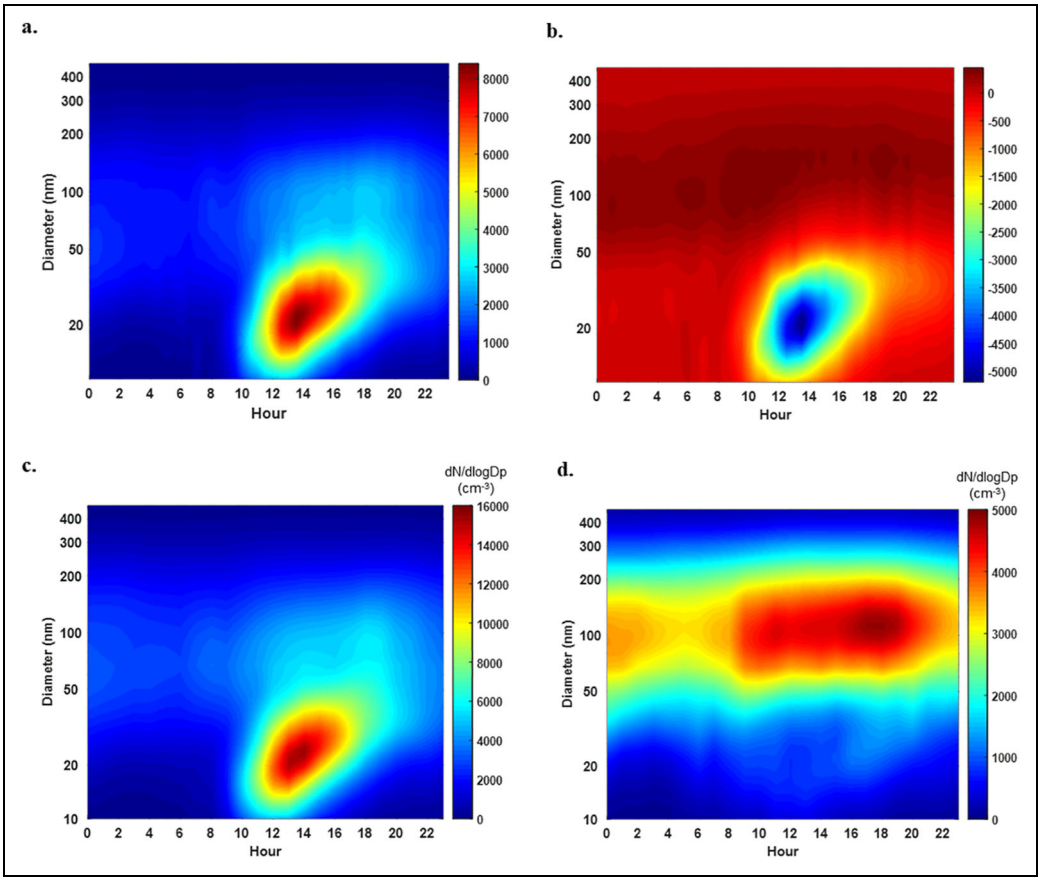

Figure 2. For the 2 main modes of empirical orthogonal function (EOF) analysis for size-separated number concentrations measured in Jeju (Aewol) from 2013 to 2016, diurnal variations in PC loadings for (a) EOF1 and (b) EOF2 and size–number distributions of ambient particles for (c) EOF1 and (d) EOF2 cases (see Section 2 for definition). Note the different color scales of the 2 EOF modes.

grew in size with a mean $GR_{10–50}$ of 2.1 ± 1.6 nm h^{-1} (growth rate [GR] of particles at 10–50 nm in diameter; **Table 1** and Text S1), which was close to the lower bound of the GR observed across China (1–15 nm h^{-1}; Chu et al., 2019, and references therein) and within the range of the global GR (1–10 nm h^{-1}; Nieminen et al., 2018, and references therein). In this case, the mean mixing ratios of gaseous precursors, such as SO_2 and NO_x, were higher by 45% and 14%, respectively, relative to the mean of the entire period (**Table 1**). In contrast, $CS_{100–470\ nm}$ (1.3 ± 0.9 × 10^{-2} s^{-1}) (**Table 1** and Text S1) was relatively lower than the mean. Thus, EOF1 was characterized by the dominant nucleation- and Aitken-mode particles and relatively high gaseous precursors and low CS, which clearly represents an NPF or at least a nanoparticle burst.

Contrary to EOF1, EOF2 was dominated by the accumulation-mode particles throughout the day (**Figure 2d**). As the number concentration of accumulation-mode particles increased in the afternoon through the evening, the maximum concentration reached 5,000 cm^{-3} at 100–130 nm; in addition, the mode of the volume concentration was found to be at larger sizes over 300 nm (Figure S3). In this case, $CS_{100–470\ nm}$ (1.8 ± 1.0 × 10^{-2} s^{-1}) was much higher but levels of gaseous precursors were comparable to EOF1 (**Table 1**). The large surface areas of pre-existing particles would strongly suppress NPF, as newly formed clusters are scavenged by pre-existing particles before reaching observable sizes of 3-nm diameters (Kulmala and Kerminen, 2008; Kulmala et al., 2017). The most evident difference between the 2 modes was the higher mass and ionic constituents of $PM_{2.5}$ in EOF2 compared to EOF1 (**Table 1**).

The 2 EOF modes are supposed to represent physically independent phenomena. If EOF1 characterizes the pattern of increase in number concentration by nucleation- and Aitken-mode particles, it is clear that EOF2 diagnoses the case where the number concentration of accumulation-mode particles increased noticeably in the absence of such small particles. However, EOF2 was rarely recognized as an episode because it does not exhibit as prominent evolution in particle number as EOF1.

3.3. Meteorological constraints and chemical consequences

The chemical properties of the 2 modes were clearly distinguished in the particle phase, including size mode, CS level, and $PM_{2.5}$ chemical compositions, but not in the gaseous precursor. Since EOF1 is much better understood as an intrinsic phenomenon for particle formation, the meteorological conditions were further delved into to elucidate EOF2 compared to EOF1.

Table 1. Characteristics of 2 modes extracted by EOF analysis of size-separated number concentrations measured in Jeju from 2013 to 2016 (mean ± 1σ)

Characteristics	Empirical Orthogonal Function 1	Empirical Orthogonal Function 2
Event	Number event	Mass event
	New particle formation (NPF)	No particle burst
Number mode diameter (nm)	<30	approximately 80–150
Growth rate$_{10–50\ nm}$ (nm h^{-1})	2.1 ± 1.6	–
Condensation sink$_{10–25\ nm}$ ($\times 10^{-2}$ s^{-1})	1.5 ± 0.9	1.9 ± 1.1
CS$_{100–470\ nm}$ ($\times 10^{-2}$ s^{-1})	1.3 ± 0.9	1.8 ± 1.0
Meteorology	Anticyclone	Synoptic-scale stagnation
Temperature (°C)	13 ± 7	16 ± 8
Relative humidity (%)	65 ± 18	73 ± 1.6
Wind direction	Northeasterly (NE 56%)	Westerly (SW 56%)
Wind speed (m s^{-1})	2.3 ± 1.6	2.7 ± 2.1
Daily solar radiation (W m^{-2})	346 ± 281	257 ± 239
Fraction of mid-low cloud (%)	40 ± 30	70 ± 30
Cloud base height (CBH, m)	1,384 ± 1,016	1,048 ± 706
Chemical constituents		
SO_2 (ppbv)	0.8 ± 0.9	0.7 ± 0.8
NO_2 (ppbv)	3.9 ± 5.1	4.0 ± 2.7
NH_3 (ppbv)	2.5 ± 3.7	2.8 ± 2.4
$PM_{2.5}$ mass (μg m^{-3})	19.1 ± 15.0	26.5 ± 21.3
SO_4^{2-} (μg m^{-3})	2.7 ± 2.8 (14%)	5.4 ± 4.7 (20%)
NO_3^- (μg m^{-3})	1.2 ± 1.9 (6%)	2.6 ± 4.1 (10%)
NH_4^+ (μg m^{-3})	1.2 ± 1.5 (6%)	2.7 ± 2.6 (10%)
$([SO_4^{2-}]+[NO_3^-])/[NH_4^+]$[a]	1.1	1.0
Sulfur oxidation ratio (SOR)[b]	0.48 ± 0.23	0.63 ± 0.24
Nitrogen oxidation ratio (NOR)[c]	0.14 ± 0.16	0.20 ± 0.19
ALWC (μg m^{-3})[d]	4.6 ± 7.9	11.6 ± 14.5
Organic carbon (OC)	3.5 ± 22 (18%)	4.1 ± 2.7 (15%)
Elemental carbon (EC)	1.0 ± 0.6 (5%)	1.2 ± 0.7 (5%)

[a] Equivalent ratio.

[b] SOR: $[SO_4^{2-}]/([SO_2] + [SO_4^{2-}])$.

[c] NOR: $[NO_3^-]/([NO_2] + [NO_3^-])$.

[d] Aerosol liquid water content (ALWC) was calculated using ISORROPIA II with forward mode.

In accordance with what has been reported previously (Dall'Osto et al., 2018; Chu et al., 2019), aerosol number–size distributions like EOF1 was frequently observed on sunny and clear days in the study region, where it was situated under a high-pressure system after frontal passage during spring and fall (Figures S2b and S4a). **Figure 3** compares the monthly characteristics of the 2 modes, including the frequency of occurrence, levels of meteorological variables, and $PM_{2.5}$ mass concentration. The latter two are given as the difference from the monthly mean. EOF1 was most evident with much lower cloud coverage (down to −60%) and much higher cloud base height (CBH, up to +800 m) than the monthly average (20–60% and 916–1,289 m, respectively) (**Figure 3**), leading to more solar radiation (SR) incoming to the surface (**Table 1**). In this period, cold and dry northerly winds prevailed (**Figures 3** and S5) and precursor gases and $PM_{2.5}$ concentrations were low compared to the mean over the entire period due to a limited contact with urban sources. Of precursor gases, SO_2 mixing ratio was slightly

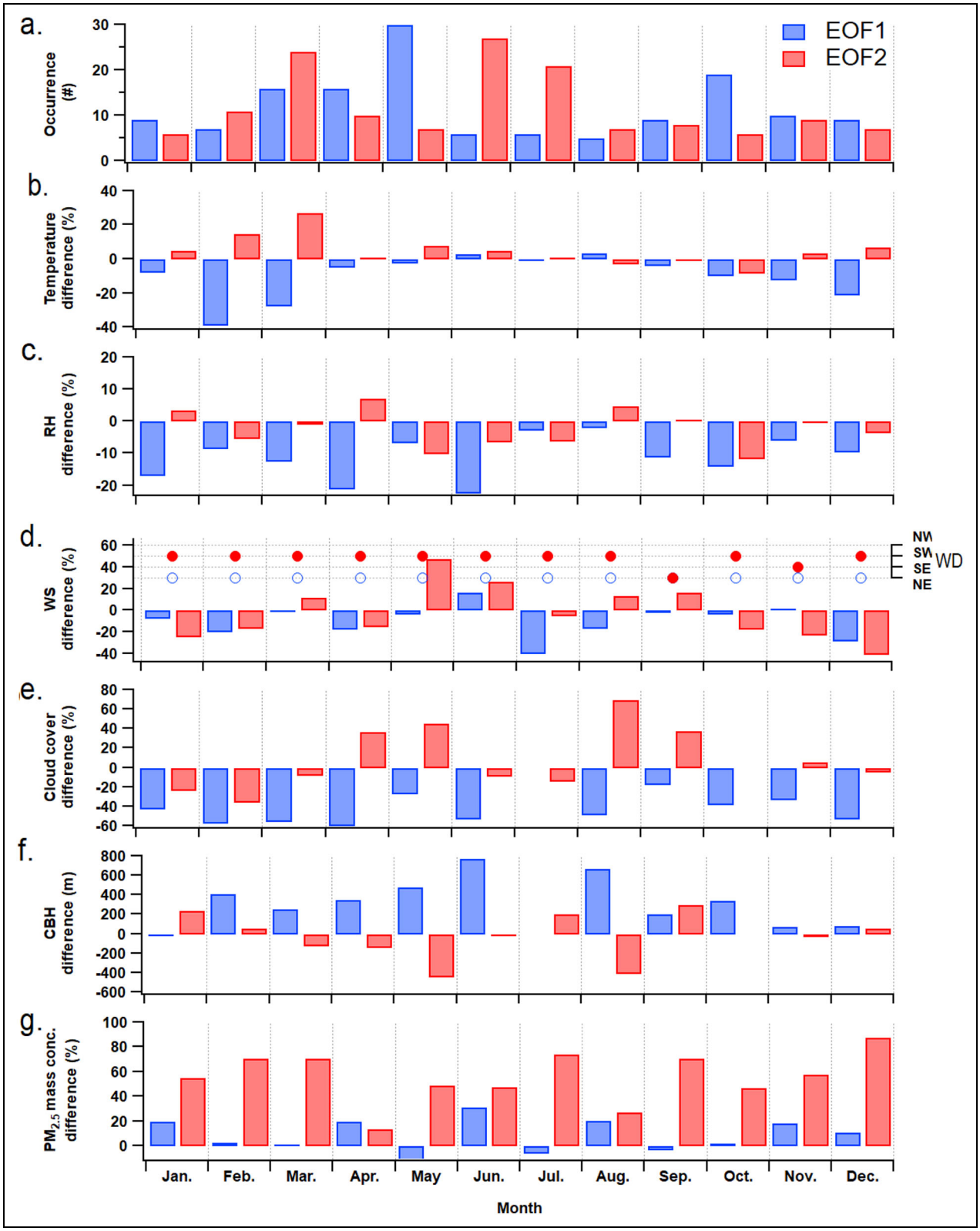

Figure 3. Monthly occurrence of the top 10% EOF1 (blue) and EOF2 (red) mode for 2013–2016 and difference of meteorological variables and $PM_{2.5}$ mass concentration from the monthly mean for the 2 modes. (a) Occurrence, (b) Temperature, (c) Relative humidity, (d) Wind speed, (e) Cloud coverage, (f) Cloud base height (CBH), and (g) $PM_{2.5}$ mass concentration.

increased in EOF1 (0–111%; 0.3–2 ppbv; Figure S6) probably from upwind sources in the continent (Wu et al., 2007; Liang et al., 2016; Tian et al., 2019). Even in March, September, and October, when both frequency and amplitudes of EOF1 was strongest (**Figures** S2 and **3**), SO_2 showed only a marginal increase (0–6%; 0.3–1.0 ppbv). Given that the particle formation has been observed to strongly depend on the abundance of sulfuric

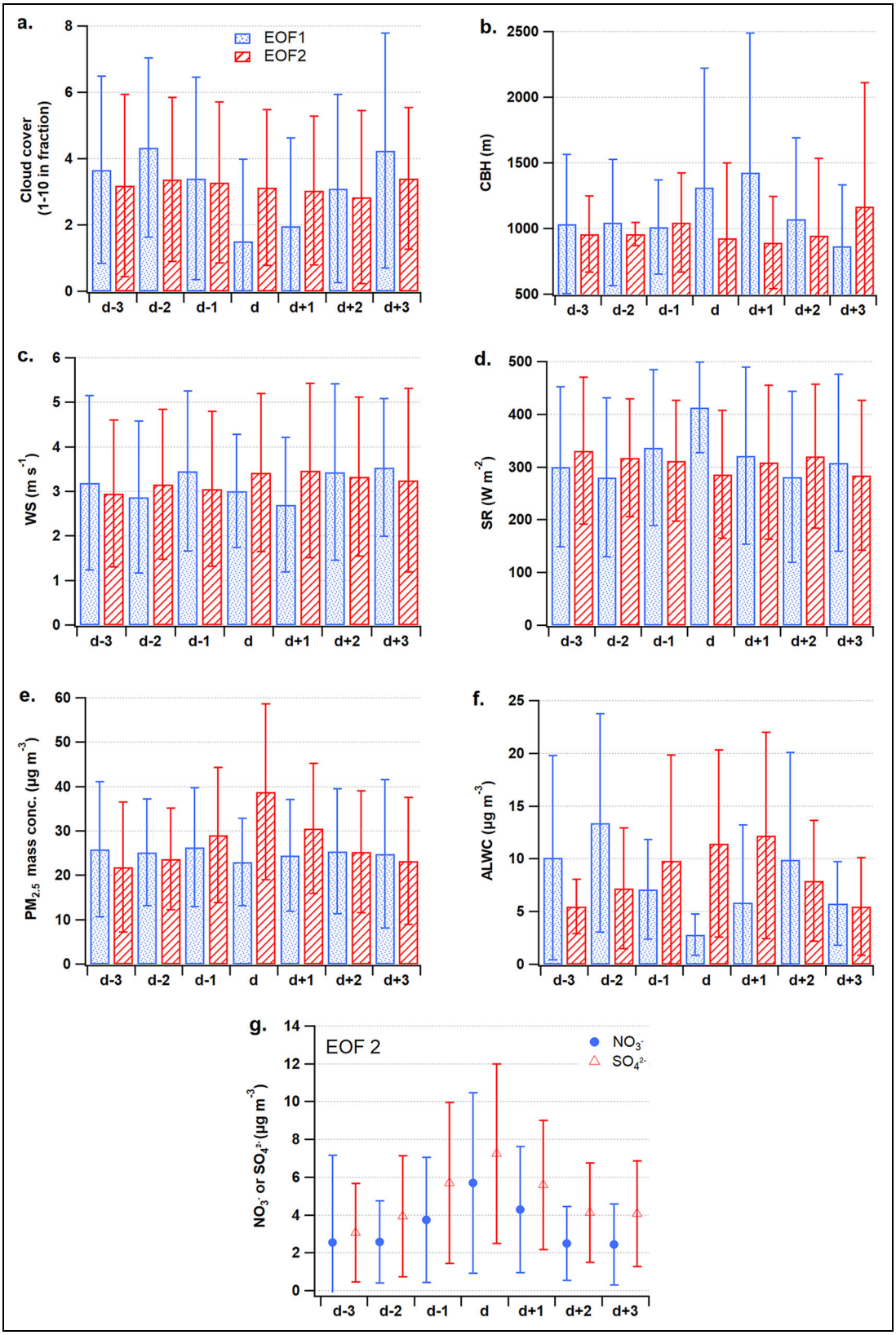

Figure 4. For EOF1 (blue) and EOF2 (red) in March for 4 years from 2013 to 2016, comparison of daily evolution of meteorological variables, $PM_{2.5}$ mass concentration, and aerosol liquid water content (ALWC) over a course of 7 days including 3 days before (d − 3 ∼ d − 1) and after (d + 1 ∼ d + 3) EOF day. (a) Cloud cover, (b) Cloud base height (CBH), (c) Wind speed (WS), (d) Incoming solar radiation (SR), (e) $PM_{2.5}$ mass concentration, and (f) Aerosol liquid water content (ALWC). In (g), variations of NO_3^- (blue) and SO_4^{2-} (red) for EOF2 are shown. Error bars indicate standard deviations.

acid (H_2SO_4) (Weber et al., 1996; Sihto et al., 2006; Hirsikko et al., 2011), our result of long-term measurements suggests that readily condensable gas concentration was somewhat insensitive to local precursor levels. In other words, the oxidation of SO_2 to H_2SO_4 is likely to be decoupled from nucleation or promoted by unidentified processes. As observed ubiquitously at midday on a regional scale, it is not surprising that NPF and subsequent growth events are sensitive to synoptic meteorological conditions and daily evolution of boundary layers, especially in East Asia (Takegawa et al., 2020).

The mean $PM_{2.5}$ concentration of EOF2 was 26.5 ± 21.3 μg m^{-3}, being higher by 40% than EOF1 (19.1± 15.0 μg m^{-3}). The $PM_{2.5}$ mass was dominated by SIA, with a mean contribution of 41% to the mass (20% SO_4^{2-}, 10% NO_3^-, 10% NH_4^+) (**Table 1**). The difference in $PM_{2.5}$ mass between the 2 modes contrasts more sharply when compared, as deviations from the monthly mean (**Figure 3g**). $PM_{2.5}$ concentrations were 14–88% higher in EOF2 than in EOF1, and the difference was 55–88% (35–39 μg m^{-3} in monthly concentration for EOF2) in cold months. Of the days exceeding the daily Korean air quality standard (35 μg m^{-3}) during the 4-year period, 29% (10%) belong to EOF2 (EOF1). Note that in the previous section, EOF2 was characterized by an increased number of accumulation mode particles. Therefore, it is reasonable to argue that EOF2 represents a distinct episode of elevated $PM_{2.5}$ mass particularly driven by high SIA mass fractions.

Contrary to EOF1, EOF2 occurred on warm, humid, and cloudy days under low CBH (**Figure 3**) and prevailing southwesterly winds blowing through the Yellow Sea (Figure S4b). The 2 modes were most clearly distinguished by cloud cover and CBH. Besides chemical mechanisms potentially operative in clouds, a mid-low CBH can be indicative of mixed layer height (MLH) particularly in the afternoon (Seidel et al., 2010; Huang et al., 2018). Hourly averaged CBH exhibits a clear diurnal variation similar to the typical MLH (Figure S7) and thus, CBH was used here as a surrogate for MLH. Then, the significantly lower CBH of EOF2 than EOF1 indicates that the boundary layer of EOF2 was much shallower than that of EOF1. A larger cloud cover was consistent with reduced SR reaching the surface in EOF2 (346 ± 281 W m^{-2} and 257 ± 239 W m^{-2} for EOF1 and EOF2, respectively: **Table 1**). However, like EOF1, $PM_{2.5}$ chemical constituents were completely neutralized (equivalent ratio of $([SO_4^{2-}] + [NO_3^-])/[NH_4^+] = 1$) with significantly elevated sulfate and nitrate oxidation ratios (SOR and NOR) (**Table 1**). Compared to the much higher SIA of EOF2 than EOF1, the difference in carbonaceous composition between the 2 modes was not significant (**Table 1**). For the 2 EOF modes, the aerosol number–size distribution was found to be closely related to the chemical composition of $PM_{2.5}$, where EOF2 was clearly distinct from EOF1. Therefore, it is highly plausible that the unique evolution of accumulation-mode particles in EOF2 was strongly associated with the increase in SIA in humid and shallow boundary layer, which eventually resulted in the $PM_{2.5}$ mass increase.

3.4. Tight coupling between aerosol phenomena and synoptic meteorology

In this study, the number–size distribution of submicron particles evolved dynamically depending on synoptic weather conditions, resulting in 2 distinct modes. EOF1 was revealed in daily evolution of particles, explicitly indicating NPF and growth events. The other mode, EOF2, was linked with an increase in $PM_{2.5}$. Recent studies have shown that individual haze pollution episodes often took place over several days (Yang et al., 2017; Tian et al., 2019; Shi et al., 2020). Therefore, changes in the key chemical and meteorological variables of the 2 modes that occurred in March over 4 years were examined over a course of 7 days including 3 days before ($d - 3 \sim d - 1$) and after ($d + 1 \sim d + 3$) EOF day (d) (**Figure 4**). Note that in March of the year, both EOF1 and EOF2 occurred frequently, and the $PM_{2.5}$ mass increase of EOF2 was also large (**Figure 3**).

In EOF2, cloud cover and CBH decreased slightly, but wind speed increased (**Figure 4a–c**) on day d. Interestingly, SR steadily decreased at a rate of −14.1 W m^{-2} day^{-1}, reaching a minimum on day d (**Figure 4d**), resulting in an inverse correlation with $PM_{2.5}$ mass concentration (**Figure 4e**). As shown above, $PM_{2.5}$ mass concentration was significantly higher on day d with a gradual increase at a rate of 5.6 μg m^{-3} day^{-1} and decrease after reaching a maximum. These progressive changes in $PM_{2.5}$, SR, and cloud properties highlight the role of $PM_{2.5}$ in reducing SR; downwelling SR was thought to be reduced by thick aerosol layer, which was dependent on aerosol size distributions and chemical composition. This finding is in agreement with a recently proposed mechanism that explains the intensified haze pollution caused by a positive feedback between increase in aerosol concentration, reduction in surface SR, and stability of boundary layer (Ding et al., 2016; Yang et al., 2016). In Beijing, this feedback effect was reported to be 15.42 W m^{-2} km^{-1}, given as a sensitivity of daily downwelling SR to visibility, where a 1 km reduction in visibility was equivalent to a 10 μg m^{-3} increase in $PM_{2.5}$ concentration (Yang et al., 2016). In this study, the combined effects of thick aerosol layer and cloud were estimated to be approximately 24 W m^{-2} per 10 μg m^{-3} for the 4 days of the EOF2 episode on average.

In **Figure 4e** and **f**, $PM_{2.5}$ mass and ALWC tend to increase simultaneously. It is noteworthy that ALWC in EOF2 continued to increase until $d + 1$, with the greatest increase during $d - 2$ and $d - 1$ (**Figure 4f**). In comparison, $PM_{2.5}$ mass increased the most between $d - 1$ and d. The increases of SO_4^{-2} and NO_3^-, which are the major constituents of $PM_{2.5}$, were similar to those of AWLC and $PM_{2.5}$, respectively (**Figure 4g**). While SO_4^{-2} steadily increased by 4.05 μg m^{-3} from $d - 3$ to d, the NO_3^- increase of 3.11 μg m^{-3} occurred between $d - 2$ and d. After d, these 2 species decreased at similar rates. During this 7-day period, RH remained high between 63% and 67% and was not correlated with ALWC. These results, therefore, indicate that SIA played a crucial role in determining ALWC, leading to a rapid increase in $PM_{2.5}$ mass. In humid atmospheric conditions with sufficient precursor gas, the conversion of water-soluble gas to particles is promoted, increasing the ALWC (Zhou et al., 2011). The

increased ALWC then shifts the partitioning of soluble gas into the particulate phase, thereby constituting a positive feedback, as reported in previous studies (Hodas et al., 2014; Xue et al., 2014; Wu et al., 2018). On d + 1, a sharp decrease in $PM_{2.5}$ with an increase in AWLC is likely to reflect scavenging of particles by hydrometeors such as mist or fog at high RH. The role of ALWC was also evident in the EOF1 event.

In EOF1, ALWC exhibited pronounced changes over 7 days with a minimum on day d. This type of variation was consistent with changes in RH, decreasing from 74% to 65% between d − 3 and d and increasing back to 72% on d + 3. In comparison, $PM_{2.5}$ concentrations varied slightly, but dropped to a minimum on day d, when cloud cover and SR showed a clear minimum (1.5 ± 2.5) and maximum (413 ± 85 W m^{-2}), respectively. As is already known, more SR boosts not only photochemical reactions but also deep vertical mixing of the boundary layer, consequently hindering SIA formation through diluting existing particles but promoting NPF and growth.

The progressive changes in meteorological and atmospheric chemical factors of the 2 EOF modes demonstrate that their interplay created the 2 distinct phenomena over a course of several days. This tight coupling allows nanoparticle formation and growth, represented by EOF1, to take place under well-constrained conditions as a standalone phenomenon. Likewise, EOF2 reflects the increase in fine aerosol mass as an episodic event occurring on a regional scale. Therefore, in the study region, EOF2 is an instance in which an increased number of accumulation-mode particles resulted in an increase in fine aerosol mass, whereas EOF1 is an event in which new particles are generated by a burst and dynamic evolution of nucleation–Aiken mode particles.

3.5. Intensive measurements during the KORUS-AQ study

In May–June 2016, the KORUS-AQ campaign was run on multiple platforms and the variety sets of measurements were made in the Korean peninsula and Northeast Asia outflow region (e.g., Crawford et al., 2021). Of several distinct episodes that occurred under distinct synoptic circulation (Peterson et al., 2019), "persistent anticyclone" and "low-level transport and haze development" episodes correspond to EOF1 and EOF2 mode, respectively, in this study. The $PM_{2.5}$ mass concentration increased in Aewol, up to 63 μg m^{-3} (**Table 2**), as well as Seoul during "transport/haze" period (Kim et al., 2018; Jordan et al., 2020), showing a regional phenomenon of the haze development. In Aewol, the aerosol number–size distributions were obviously different during these 2 periods (**Figure 5**). Hereafter, the 2 distinct periods during the campaign referred to as "persistent anticyclone" and "transport/haze" periods, respectively, which were compared for meteorological and chemical properties in subsequent sections (**Table 2**).

3.6. Increase in accumulation mode particles from vertical observation

The high surface temperature resulted in a deep mixing layer on May 20 of "persistent anticyclone" period (**Figure 6a**). The particle number concentrations at all size ranges were low over the altitude, explained by dilution of preexisting particles by vertical mixing. In contrast, in the morning on May 25 ("transport/haze" period), the mixed layer was shallow with a temperature inversion layer at about 1,000 m (top gray box in **Figure 6b**). The morning profile illustrates visibly high concentrations of the $particle_{3.5\ nm–0.3\ \mu m}$ (about 10^4 cm^{-3}) both at surface and at around the inversion (gray boxes in **Figure 6h**). The high concentration near the surface is attributed to fresh emissions in the morning. On the other hand, high number of $particle_{3.5\ nm–0.3\ \mu m}$ at around the inversion is similar to the results of previous studies in which a large number of ultrafine particles were commonly found above the cloud as a result of an enhanced photochemical reaction (Clarke, 1993). In the afternoon, the thin layer laden with large amount of $particle_{3.5\ nm–0.3\ \mu m}$ disappeared, but the number of accumulation mode particles ($particle_{0.3–0.5\ \mu m}$ and $particle_{0.5–1.0\ \mu m}$) increased remarkably, particularly at altitudes between 1,000–1,500 m (**Figure 6i**). It is evident for the evolution of nucleation- and Aitken-mode particles existing in the inversion layer, as the PBL developed.

In urban areas with heavy local emissions, a strong inversion forces the local circulation to be confined to the atmospheric boundary layer under undesirable ventilation, thereby acting as a lid; thus, pollutants are accumulated within the boundary layer (e.g., Ye et al., 2016; Ning et al., 2018). In contrast to the heavily polluted sites, in the background or outflow sites, the significant elevation in aerosol concentration during the day is believed to occur primarily by the intrusion of pollutants carried from the upper atmospheric layer, for example, residual layer formed at night or free troposphere, upon the expansion of the PBL. Evidently, the concentrations of $PM_{2.5}$ and all gaseous precursors increased during the daytime when the PBL expanded (Figure S7) and the wind direction was shifted to a westerly flow (Figure S5). Recently, it was suggested that pollutants were carried from the upstream areas in the upper layer by westerly winds, remained above the nocturnal boundary layer, and entrained into the PBL during the day; this led to a high PM_{10} concentration at the surface of Seoul (Lee et al., 2019). The $PM_{2.5}$ haze pollution was accompanied with a strong temperature inversion in downwind regions of polluted Northeast China (Shi et al., 2020). Therefore, these results indicate that the rapid increase in $PM_{2.5}$ mass in Northeast Asia could be closely coupled with the development of the PBL.

In more detail, the vertical profiles indicate that the particle number concentrations correlated with changes in ambient RH (**Figure 6**). Compared to the "persistent anticyclone" period with a deep vertical mixing and dilution, "transport/haze" period was characterized by discernable layers of the vertical structure of meteorological variables including RH, temperature, and wind direction. Such a shallow boundary layer of high RH is favorable for gas-to-particle conversion and hygroscopic growth of particles, thereby greatly affecting the concentration and size distribution of particles. We considered the deliquescence relative humidity (DRH) of inorganic salts, such as NH_4NO_3 and $(NH_4)_2SO_4$, as a crucial factor

Table 2. Comparison of 2 distinct episodes that occurred during the 2016 KORUS-AQ campaign corresponding to the 2 EOF modes

Episodes	Persistent Anticyclone May 18–20, 2016	Low-Level Transport and Haze Development May 25–27, 2016
EOF mode	EOF1: NPF observed	EOF2: $PM_{2.5}$ mass increase observed
Meteorology		
Temperature (°C)/RH (%)	18 ± 4/53 ± 9	18 ± 3/73 ± 13
Wind direction[a]/speed (m s^{-1})	Easterly/1.6 ± 0.9	Westerly/1.2 ± 0.6
Boundary layer: depth/inversion/stability	Deep/weak/unstable	Shallow/strong/stable
Free troposphere: temperature/winds	Low/weak northerly	High/strong westerly
Aerosol size–number distribution		
Number mode diameter (nm)	<60	approximately 100
Volume mode diameter (nm)	198-305	305-470
rBC properties		
Mass concentration (μg m^{-3})	0.4 ± 0.1	0.6 ± 0.2
Count mode diameter (CMD) (nm)	90	110
Mass mode diameter (MMD) (nm)	200	220
Coating thickness (nm)[a] (mean ± 1 σ, 50th, 75th)	29 ± 31, 20, 40	48 ± 39, 40, 75
Chemical constituents		
SO_2 (ppbv)	1.0 ± 0.4	0.7 ± 0.4
NO_2 (ppbv)	7.0 ± 2.1	4.3 ± 1.6
NH_3 (ppbv)	3.4 ± 8.7	3.8 ± 2.4
$PM_{2.5}$ mass (μg m^{-3})	14.3 ± 5.9	34.5 ± 13.1 (max: 63.0)
SO_4^{2-} (μg m^{-3})	0.7 ± 0.5	6.2 ± 2.7
NO_3^- (μg m^{-3})	0.1 ± 0.2	1.1 ± 1.2
NH_4^+ (μg m^{-3})	0.3 ± 0.3	3.3 ± 1.4
$([SO_4^{2-}] + [NO_3^-]) / [NH_4^+]$[b]	1.0	0.8
ALWC (μg m^{-3})	0.9 ± 0.3	10.3 ± 8.2
Organic carbon (OC)	3.8 ± 1.3	4.1 ± 1.7

[a] Restricted to 180 nm $\leq D_{rBC} \leq$ 220 nm; coating defined as coating thickness $\geq$10 nm considering systematic uncertainty (Laborde et al., 2013).

[b] Equivalent ratio.

for the rapid particle growth, because the SIA was the predominant constituent of $PM_{2.5}$ observed during the KORUS-AQ period (Jordan et al., 2020) as well as in Aewol for 4 years. In the morning, the burst of $particle_{3.5\ nm–0.3\ \mu m}$ above 10^4 cm^{-3} occurred at altitudes with RH below the DRHs of both $(NH_4)_2SO_4$ and NH_4NO_3 (**Figure 6b** and **h**). This layered structure became uniform in the afternoon with the expansion the PBL coinciding with elevated RH around the DRH of both $(NH_4)_2SO_4$ and NH_4NO_3, resulting in a noticeable reduction of $particle_{3.5\ nm–0.3\ \mu m}$ and an increase of $particle_{0.3–0.5\ \mu m}$ and $particle_{0.5–1.0\ \mu m}$ in number concentration at altitudes between 1,000 m and 1,500 m (**Figure 6c** and **h**). It is likely that the mixing through inversion layer caused hygroscopic growth of existing nucleation- and Aitken-mode particles, which led to an increase in the number of accumulation-mode particles where the water-soluble vapors readily condensed, adding mass to the particles.

Therefore, the vertical profiles of aerosol number concentrations and their evolution during "transport and haze development" period suggest that (1) the entrainment of nanoparticles from the upper layer into the shallow and humid boundary layer with locally emitted or transported precursors and condensable gases, (2) the evolution of nanoparticles to accumulation-mode particles by increase in size via hygroscopic growth and mass via gas-to-particle conversion, and (3) consequently, the contribution of accumulation-mode particles to increase in $PM_{2.5}$ mass. Given that the synoptic circulation is the main deriver determining the level of atmospheric constituents over

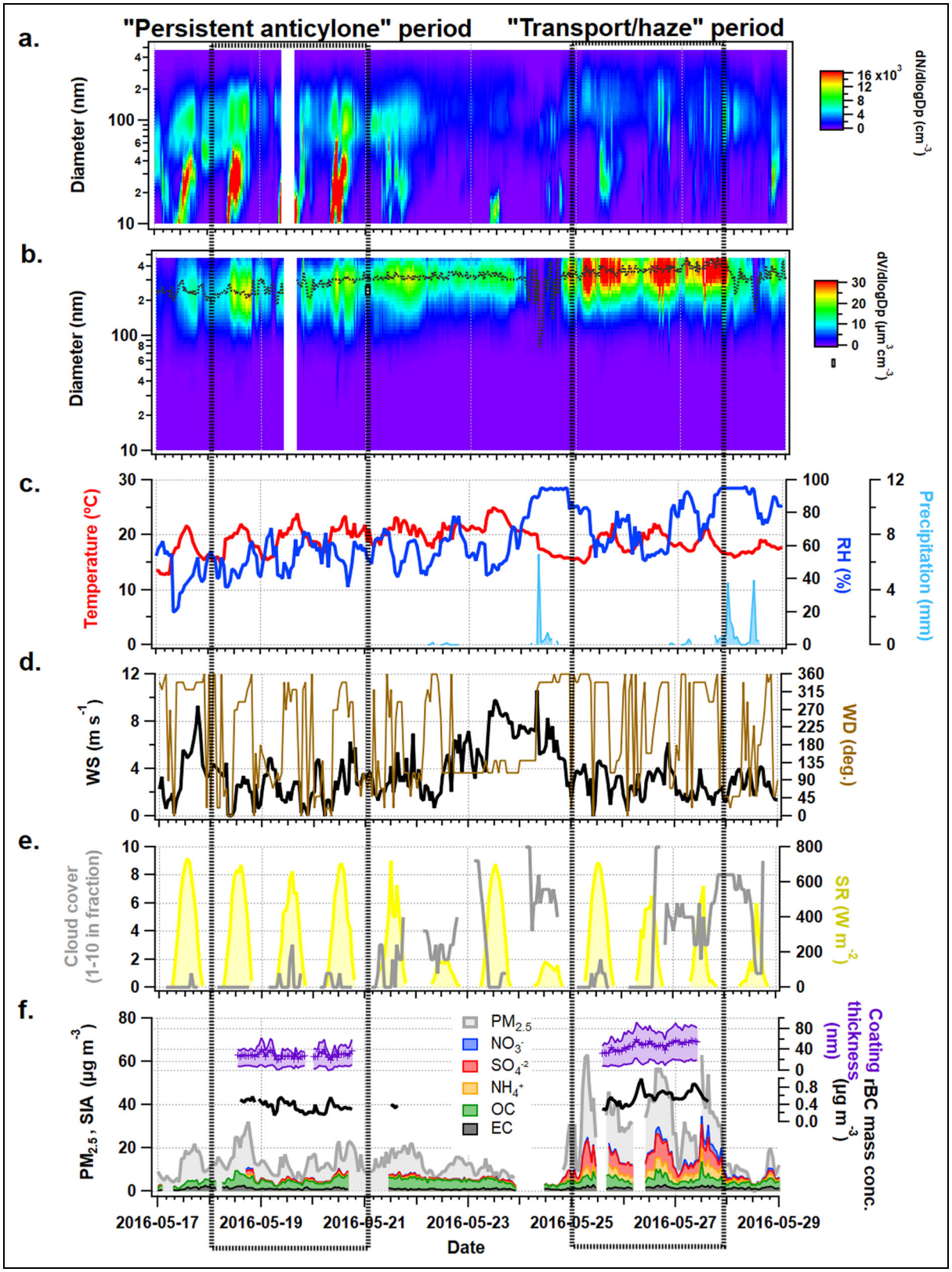

Figure 5. Time-series of aerosol properties and meteorological variables measured in Jeju during the 2016 KORUS-AQ campaign. Two distinct episodes referred to as "persistent anticyclone (May 18–20)" and "transport/haze (May 25–27)" correspond to EOF1 and EOF2, respectively (indicated by black boxes). (a) Aerosol number–size distribution, (b) Aerosol volume size distribution with peak diameter every 30 min (black dotted line), (c) Temperature (red), relative humidity (RH; blue), and precipitation (sky blue), (d) Wind speed (WS) and wind direction (WD), (e) Cloud cover and solar radiation (SR), and (f) $PM_{2.5}$ and secondary inorganic aerosol (SIA) mass concentration, and rBC mass concentration (black) and coating thickness (purple; hourly mean, 25th, and 75th percentiles).

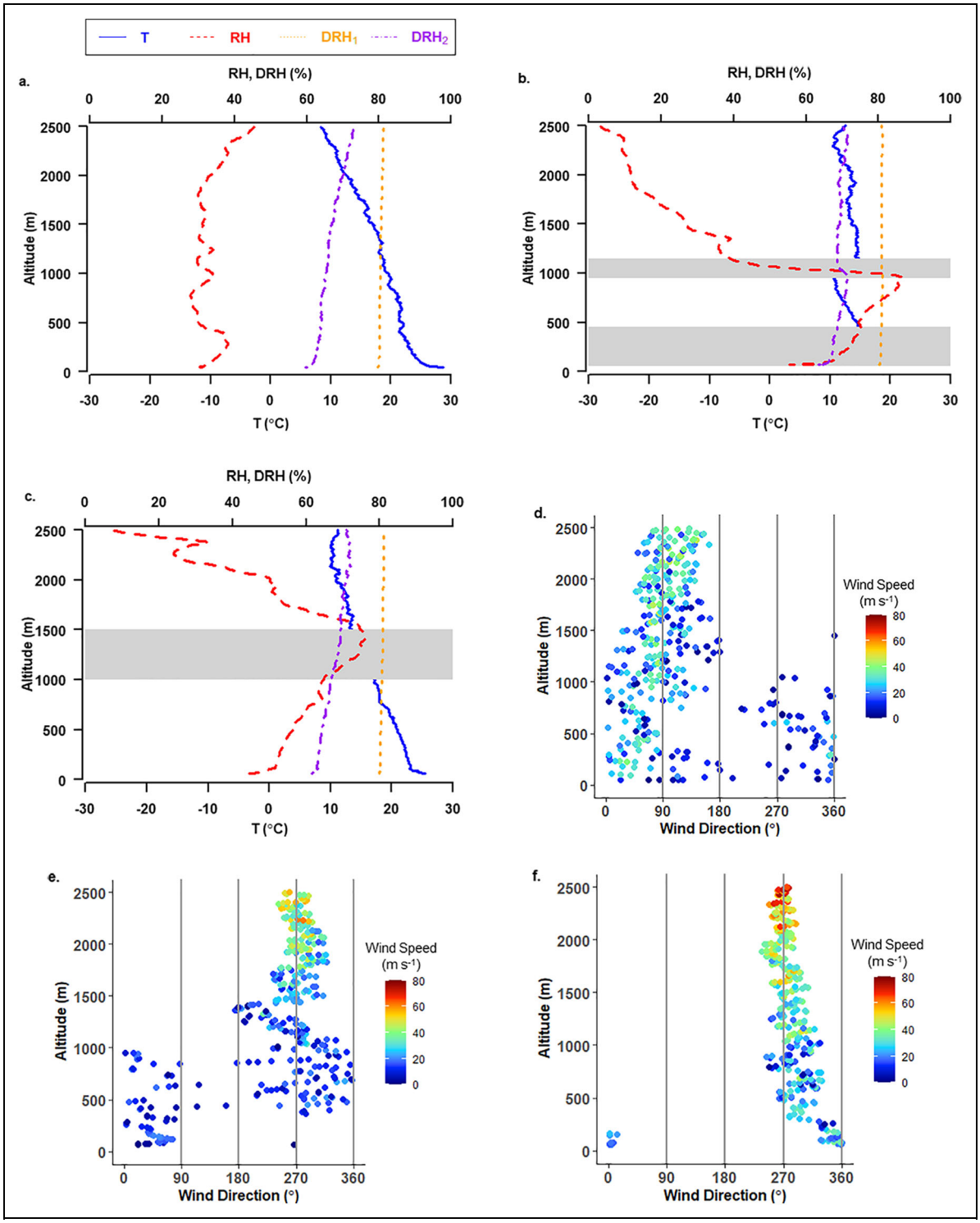

Figure 6. Vertical distributions of meteorological variables and aerosol number concentrations observed in Seoul Metropolitan Area (SMA) during the 2016 KORUS-AQ campaign. (a), (d), (g) In the morning on 20 May during "persistent anticyclone" period, and (b), (e), (h) in the morning and (c), (f), (i) afternoon on 25 May during "low-level transport and haze development" period. The panel (a), (b), (c) presents temperature (solid blue), RH (dotted red), and deliquescence RH of NH_4NO_3 (sky blue) and $(NH_4)_2SO_4$ (green). The panel (d), (e), (f) presents WD color-coded by WS (m s^{-1}). The panel (g), (h), (i) number concentrations (cm^{-3}) of $particle_{3.5\ nm–0.3\ \mu m}$ between 3.5 nm and 0.3 μm in diameter (green), $particle_{0.3–0.5\ \mu m}$ between 0.3 μm and 0.5 μm (purple), and $particle_{0.5–1.0\ \mu m}$ between 0.5 μm and 1.0 μm (yellow). Point measurement data are shown as open circles (gray) and mean ± standard deviation are given as closed circles for every 500 m altitude. In (i), the vertical profiles of (h) are overlayed (light gray). The altitude ranges discussed in the text are shaded by color.

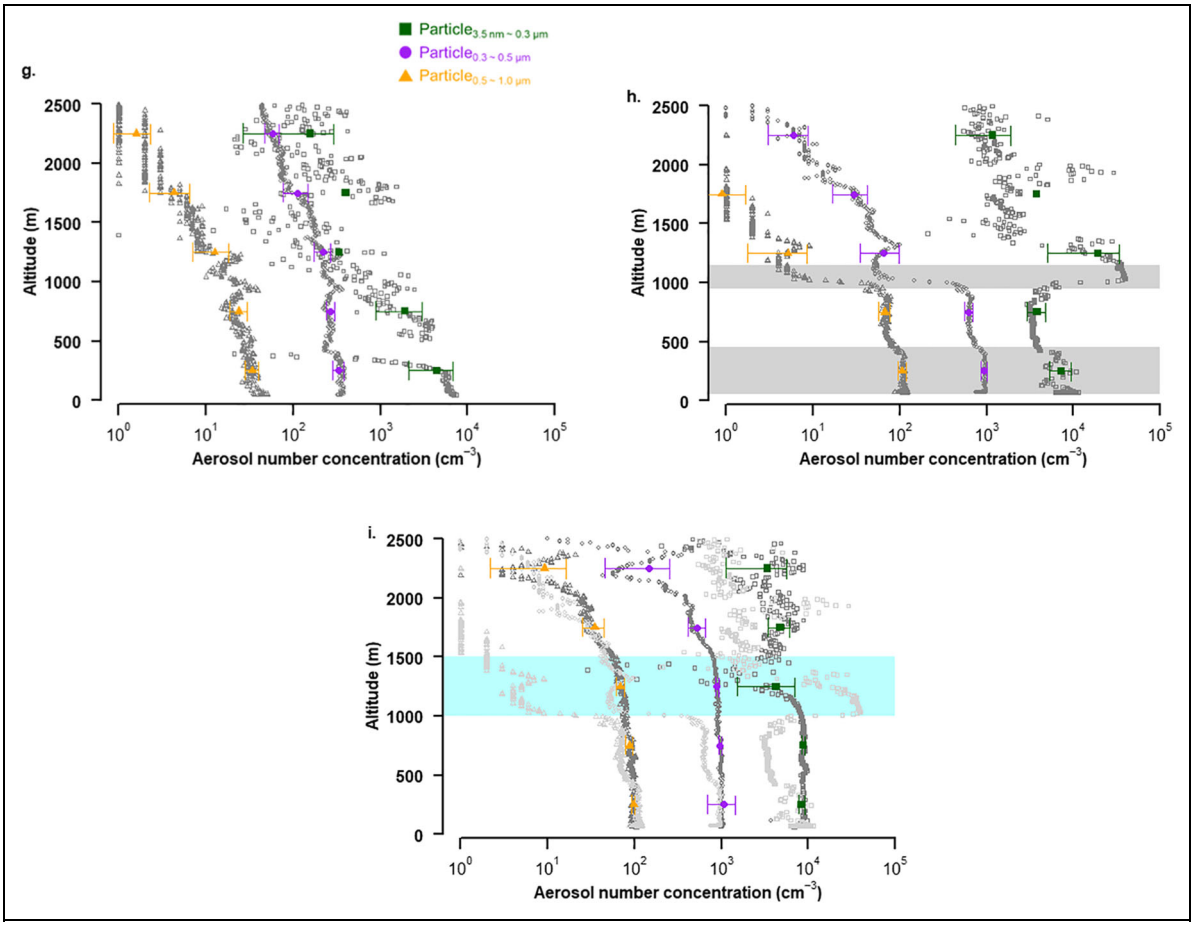

Figure 6. (Continued).

the Korean peninsula (Peterson et al., 2019; Jordan et al., 2020), this process would have been active for $PM_{2.5}$ mass increase throughout EOF2 periods.

3.7. rBC as a robust tracer for particle growth in size and mass

In addition to the evolution of nanoparticles, the role of accumulation-mode particles in increasing the aerosol mass was highlighted above. Among aerosol particles, BC is of particular interest, as bare BC particle is insoluble and small, generally peaking below 100 nm in number and thus it potentially provides a chemically inert surface on which volatile substances can condense to form a coating and further grow on. In terms of climate effect, BC has been well established as the significant warming agent (Bond et al., 2013). To assess a role of BC particle in aerosol transformation, the mass and mixing state of rBC particles were determined at GCO in Jeju and compared between the 2 periods of the KORUS-AQ campaign ("persistent anticyclone" and "transport/haze") (**Table 2**; **Figures 5f** and **7**).

Figure 7a illustrates variations of D_{shell} (optical diameter of rBC-containing particle in a core-shell configuration with rBC core restricted to 180–220 nm; Section 2.1) as a function of $PM_{2.5}$ concentration for the entire campaign period. D_{shell} increased almost linearly with $PM_{2.5}$ mass concentration, reaching 300–400 nm on average at $PM_{2.5}$ higher than 40 μg m^{-3}. This reveals a close relationship between rBC coating thickness and $PM_{2.5}$ mass enhancements. In **Figure 7b**, volume concentration of $particles_{200–470\ nm}$ was also elevated simultaneously with $PM_{2.5}$ mass concentrations, and rBC coating was obviously thicker (48 ± 39 nm) during "transport/haze" period when the $PM_{2.5}$ mass concentration was highly elevated over the Korean peninsula (Jordan et al., 2020). These results demonstrate that rBC-containing particles with thick coatings are truly representative of accumulation-mode particles in terms of size particularly during "transport/haze" period. Together with the enhanced SIA concentrations and the thicker coating of rBC (**Figure 7b** and **c**), ALWC was as high as 10.3 ± 8.2 μg m^{-3}, accounting for 30% of the dry $PM_{2.5}$ mass (**Figure 7c**; **Table 2**). Given that the RH remained high at greater than 60% during the day and up to 90% at night (**Figure 7b**), hygroscopic growth of NH_4NO_3 and $(NH_4)_2SO_4$ by uptake of water was expected to be promoted, leading to a large increase in ALWC. SOR was almost linearly increased with RH (Figure S8b and d). More importantly, sulfuric acid is known to readily condense on the rBC surface (Zhang et al., 1993; Zhang et al., 2008; Kiselev et al., 2010), which provides an active surface for heterogeneous reaction by changing its hygroscopic properties (Khalizov et al., 2009). Hence, the characteristic features observed during the "transport/haze" period suggest an effective condensation of vapors to rBC surfaces and reaction with SIA, resulting subsequent growth of rBC particles in size and

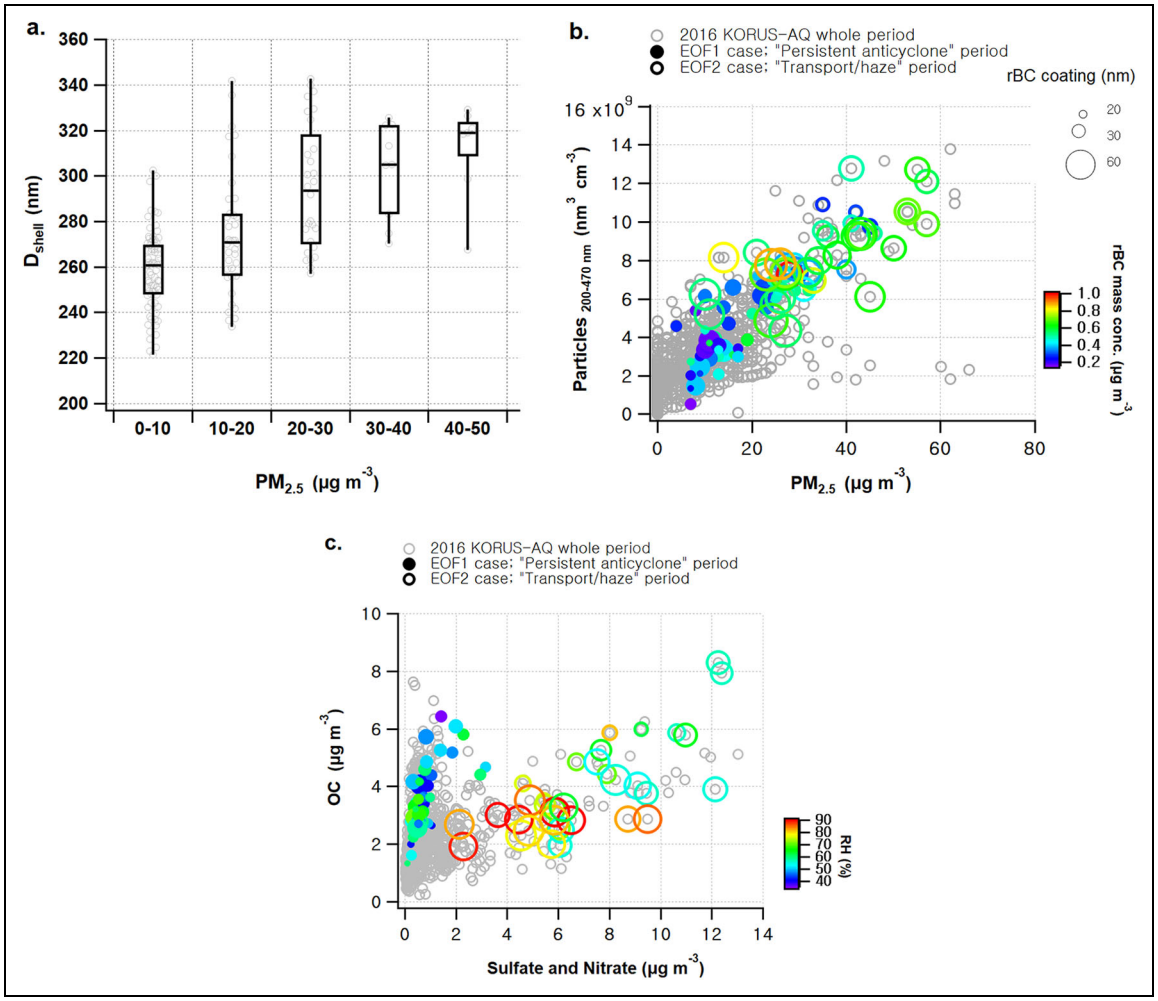

Figure 7. Relationships of rBC properties, $PM_{2.5}$ mass and composition, and particles$_{200–470}$ volume concentration measured during the KORUS-AQ campaign. (a) The variation of the diameter of shell (D_{shell}) as a function of $PM_{2.5}$ concentration for the entire campaign period, (b) the relationship between particles$_{200–470}$ volume concentration and $PM_{2.5}$ mass concentration color-coded by rBC mass concentration, and (c) the relationship between $PM_{2.5}$ chemical constituents color-coded by RH. In (a), the box plot is read as follows: the upper and lower boundaries of the box indicate the 75th and the 25th percentiles, the line within the box marks the median, and the whiskers above and below the box denote the 90th and 10th percentiles for each $PM_{2.5}$ bin. In (b) and (c), the marker size is proportional to the rBC coating thickness. D_{shell} and coating thickness are restricted to 180 nm $\leq$ diameter of rBC core (D_{rBC}) $\leq$ 220 nm.

mass by forming thick coating on their surfaces (Adachi et al., 2014; Ueda et al., 2016; Lim et al., 2018). The shell size of rBC with a core diameter of 180–220 nm reached approximately 300–400 nm. Given that the $PM_{2.5}$ concentration increased linearly with the volume concentration of particles$_{200–470\ nm}$ (**Figure 7a**), the role of internally mixed BC particles is critical to the increase in mass of fine aerosol, as they provide surfaces for gaseous precursors of SIA to condense on.

In contrast, a thinner coating (29 $\pm$ 31 nm) and a lower concentration (by 40%) of rBC particles as well as the low levels of SIA were evident under low RH (53 $\pm$ 9%) conditions during "persistent anticyclone" period. In this case, the organic carbon (OC) fraction was the greatest in $PM_{2.5}$. ALWC was very low as well, possibly due to less water uptake by the aged organic aerosol (Engelhart et al., 2011). It is likely that meteorological conditions suppressed the condensation of volatile materials on aerosol surface and thus the secondary aerosol formation on rBC surface. It is also possible that organic materials may form an organic film on the BC surface, inhibiting the vapor uptake for SIA and the increase in rBC coating (Saxena et al., 1995; Sellegri et al., 2003). Instead, they promoted the growth of nucleation- and Aitken-mode particles smaller than 60 nm under low RH conditions (**Figure 7a**). The mass size distributions of OC, NO_3^-, and SO_4^{-2} estimated by the aerosol mass spectrometer generally show organics enriched in nucleation-mode particles (e.g., Kang et al., 2018; Kim et al., 2018).

In this regard, rBC particles and their coating thickness are proposed as an agent for generating accumulation-mode particles through SIA formation and as an operational parameter to understand the chemical mechanisms responsible for fine aerosol pollution driven by SIA,

respectably. This, in turn, implies that reducing primary emissions of gaseous precursors and small particulates such as BC will be one of the effective ways to combat high $PM_{2.5}$ mass concentrations in Northeast Asia, especially during the cold months.

4. Conclusions

In Jeju, a background site in Northeast Asia, a 4-year (2013–2016) data set of nanoparticle distributions, $PM_{2.5}$ chemical composition, gaseous precursors, and meteorological variables were analyzed together with the vertical profiles of aerosol number concentrations and rBC properties that were measured during the KORUS-AQ study in 2016.

An EOF analysis of the size-separated number distribution distinguished 2 modes of aerosol diurnal evolution: the burst in nucleation- and Aitken-mode (EOF1) and the dominant number loadings in accumulation-mode (EOF2) particles. Our 4-year measurements at a regional background site highlights that EOF2 is representative of an episodic event diagnosing $PM_{2.5}$ mass increase that occurs over a course of several days, constrained by persistent clouds and shallow boundary layer, but not coupled with the NPF and growth event. Moreover, our results of SIA-driven $PM_{2.5}$ increases support previously proposed hypothesis about dynamic interactions between aerosol loading and meteorological parameters, that is, enhanced particle loading and reduced SR in the boundary layer, and SIA formation and ALWC enhancement.

Analyses of measurements obtained during the KORUS-AQ provided insight into the processes involved in the increase of $PM_{2.5}$ mass in this region; nanoparticles were entrained into the shallow boundary layer upon vertical mixing and gases condensed onto these particles at high RH exceeding the DRH of major inorganic salts, leading to an increase in $PM_{2.5}$ mass. RH played a critical role in this process and ALWC reached 30% of the dry $PM_{2.5}$ mass. Moreover, the first measurement set of rBC properties in Jeju demonstrates convincing evidence that BC particles provide surfaces for precursor gases to condense and form coating on, facilitating an increase in aerosol size and mass, particularly in the accumulation-mode. As a result, the coating thickness of rBC is hypothesized to serve as a proxy indicating the occurrence of SIA-driven high $PM_{2.5}$ mass in the study region. Consequently, our result supports strategies for reducing primary emissions of gaseous precursor for secondary inorganic species and rBC particles that provide the co-benefits of mitigating fine aerosol pollution and climate change. Detailed mechanism of heterogeneous reaction involving BC particles needs to be addressed in the future research.

Data accessibility statement

The meteorological data compiled by Korean Meteorological Administration are available online at https://data.kma.go.kr/resources/html/en/aowdp.html (Last access: July 3, 2022). The long-term measurements made in Jeju by National Institute for Environmental Research (Jeju Aewol 2013-2016), along with vertical measurements of aerosol size distributions (Vertical Particle# Ansan May 2016 KORUS) and black carbon measurements (rBC Mixing state Jeju May 2016 KORUS) are available at KUPMO3 (https://sites.google.com/korea.ac.kr/kumpo3/home; Last access: July 31, 2022).

Supplemental files

The supplemental files for this article can be found as follows:

Text S1. Figures S1–S8. PDF

Funding

This research was supported by the National Research Foundation of Korea (NRF), funded by the Ministry of Science and ICT (MSIT) (NRF2020M3G1A111499813). S. Lim was supported by the National Research Foundation of Korea (NRF) from the Ministry of Science and ICT (2018R1D1A1B07050849 and 2021R1C1C2011543). M. Lee thanks to the support by the National Research Foundation of Korea (NRF) funded by the Ministry of Science and ICT (NRF2020R1A2C301459213). S.-W. Kim was supported by the Basic Science Research Program through the National Research Foundation of Korea (NRF), funded by the Ministry of Education (2017R1D1A1B06032548). Funding to K.-S. Kang was provided by the National Institute of Environmental Research (NIER-RP2017-166).

Competing interests

The authors declare no competing financial interest.

Author contributions

Contributed to conception and design: SL, ML, XS.

Contributed to acquisition of data: SL, ML, PL, SK, KA, JG, MZ, KK.

Contributed to analysis and interpretation of data: SL, ML, KA, XS, JG, MZ, KK.

Drafted and/or revised the article: SL, ML, PL, SK.

Approved the submitted version for publication: SL, ML, PL.

References

Adachi, K, **Zaizen, Y**, **Kajino, M**, **Igarashi, Y.** 2014. Mixing state of regionally transported soot particles and the coating effect on their size and shape at a mountain site in Japan. *Journal of Geophysical Research: Atmospheres* **119**(9): 5386–5396. DOI: http://dx.doi.org/10.1002/2013JD020880.

An, H, **Han, J**, **Lee, M**, **Kang, E.** 2015. The long-term variations of ozone and nitrogen oxides in Suwon city during 1991–2012. *Korean Society for Atmospheric Environment* **31**(4): 378–384. DOI: http://dx.doi.org/10.5572/KOSAE.2015.31.4.378.

An, Z, **Huang, R-J**, **Zhang, R**, **Tie, X**, **Li, G**, **Cao, J**, **Zhou, W**, **Shi, Z**, **Han, Y**, **Gu, Z**, **Ji, Y.** 2019. Severe haze in northern China: A synergy of anthropogenic emissions and atmospheric processes. *Proceedings of the National Academy of Sciences of the United States of America* **116**(18): 8657–8666. DOI: http://dx.doi.org/10.1073/pnas.1900125116.

Apte, JS, **Brauer, M**, **Cohen, AJ**, **Ezzati, M**, **Pope, CA.** 2018. Ambient $PM_{2.5}$ reduces global and regional

life expectancy. *Environmental Science & Technology Letters* **5**(9): 546–551. DOI: http://dx.doi.org/10.1021/acs.estlett.8b00360.

Atkinson, RW, **Mills, IC**, **Walton, HA**, **Anderson, HR.** 2015. Fine particle components and health—A systematic review and meta-analysis of epidemiological time series studies of daily mortality and hospital admissions. *Journal of Exposure Science and Environmental Epidemiology* **25**(2): 208–214. DOI: http://dx.doi.org/10.1038/jes.2014.63.

Baumgardner, D, **Popovicheva, O**, **Allan, J**, **Bernardoni, V**, **Cao, J**, **Cavalli, F**, **Cozic, J**, **Courcoux, Y**, **Diapouli, E**, **Eleftheriadis, K**, **Genberg, PJ**, **Gonzalez, C**, **Gysel, M**, **John, A**, **Kirchstetter, TW**, **Kuhlbusch, TAJ**, **Laborde, M**, **Lack, D**, **Müller, T**, **Niessner, R**, **Petzold, A**, **Piazzalunga, A**, **Putaud, JP**, **Schwarz, J**, **Sheridan, P**, **Subramanian, R**, **Swietlicki, E**, **Valli, G**, **Vecchi, R**, **Viana, M**. 2012. Soot reference materials for instrument calibration and intercomparisons: A workshop summary with recommendations. *Atmospheric Measurement Techniques* **5**(2): 1869–1887. DOI: http://dx.doi.org/10.5194/amtd-5-2315-2012.

Bertram, TH, **Thornton, JA.** 2009. Toward a general parameterization of N_2O_5 reactivity on aqueous particles: The competing effects of particle liquid water, nitrate and chloride. *Atmospheric Chemistry and Physics* **9**(21): 8351–8363. DOI: http://dx.doi.org/10.5194/acp-9-8351-2009.

Bertram, TH, **Thornton, JA**, **Riedel, TP**, **Middlebrook, AM**, **Roya, B**, **Bates, TS**, **Quinn, PK**, **Coffman, DJ.** 2009. Direct observations of N_2O_5 reactivity on ambient aerosol particles. *Geophysical Research Letters* **36**(19): 19803. DOI: http://dx.doi.org/10.1029/2009GL040248.

Bond, TC, **Doherty, SJ**, **Fahey, DW**, **Forster, PM**, **Berntsen, T**, **DeAngelo, BJ**, **Flanner, MG**, **Ghan, S**, **Kärcher, B**, **Koch, D**, **Kinne, S**, **Kondo, Y**, **Quinn, PK**, **Sarofim, MC**, **Schultz, MG**, **Schulz, M**, **Venkataraman, C**, **Zhang, H**, **Zhang, S**, **Bellouin, N**, **Guttikunda, SK**, **Hopke, PK**, **Jacobson, MZ**, **Kaiser, JW**, **Klimont, Z**, **Lohmann, U**, **Schwarz, JP**, **Shindell, D**, **Storelvmo, T**, **Warren, SG**, **Zender, CS**. 2013. Bounding the role of black carbon in the climate system: A scientific assessment. *Journal of Geophysical Research: Atmospheres* **118**(11): 5380–5552. DOI: http://dx.doi.org/10.1002/jgrd.50171.

Bond, TC, **Habib, G**, **Bergstrom, RW.** 2006. Limitations in the enhancement of visible light absorption due to mixing state. *Journal of Geophysical Research: Atmospheres* **111**(D20): D20211. DOI: http://dx.doi.org/10.1029/2006JD007315.

Boucher, O, **Randall, D**, **Artaxo, P**, **Bretherton, C**, **Feingold, G**, **Forster, P**, **Kerminen, V-M**, **Kondo, Y**, **Liao, H**, **Lohmann, U**, **Rasch, P**, **Satheesh, SK**, **Sherwood, S**, **Stevens, B**, **Zhang, XY**. 2013. Clouds and aerosols, in Stocker, TF, Qin, D, Plattner, G-K, Tignor, M, Allen, SK, Doschung, J, Nauels, A, Xia, VBY, Midgley, PM eds., *Climate change 2013: The physical science basis. Contribution of Working Group I to the Fifth Assessment Report of the Intergovernmental Panel on Climate Change*. New York, NY: Cambridge University Press: 571–657. DOI: http://dx.doi.org/10.1017/CBO9781107415324.016.

Burnett, R, **Chen, H**, **Szyszkowicz, M**, **Fann, N**, **Hubbell, B**, **Pope, CA**, **Apte, JS**, **Brauer, M**, **Cohen, A**, **Weichenthal, S**, **Coggins, J**, **Di, Q**, **Brunekreef, B**, **Frostad, J**, **Stephen, SL**, **Kan, H**, **Katherine, DW**, **George, DT**, **Richard, BH**, **Chris, CL**, **Michelle, CT**, **Jerrett, M**, **Krewski, D**, **Susan, MG**, **Diver, WR**, **Ostro, B**, **Goldberg, D**, **Daniel, LC**, **Randall, VM**, **Peters, P**, **Pinault, L**, **Tjepkema, M**, **Donkelaar, AV**, **Paul, JV**, **Anthony, BM**, **Yin, P**, **Zhou, M**, **Wang, L**, **Nicole, AHJ**, **Marra, M**, **Richard, WA**, **Tsang, H**, **Thach, TQ**, **John, BC**, **Ryan, TA**, **Jaime, EH**, **Laden, F**, **Cesaroni, G**, **Forastiere, F**, **Weinmayr, G**, **Jaensch, A**, **Nagel, G**, **Concin, H**, **Joseph, VS**. 2018. Global estimates of mortality associated with long-term exposure to outdoor fine particulate matter. *Proceedings of the National Academy of Sciences of the United States of America* **115**(38): 9592–9597. DOI: http://dx.doi.org/10.1073/pnas.1803222115.

Cai, W, **Li, K**, **Liao, H**, **Wang, H**, **Wu, L.** 2017. Weather conditions conducive to Beijing severe haze more frequent under climate change. *Nature Climate Change* **7**(4): 257–262. DOI: http://dx.doi.org/10.1038/nclimate3249.

Chu, B, **Kerminen, V-M**, **Bianchi, F**, **Yan, C**, **Petäjä, T**, **Kulmala, M.** 2019. Atmospheric new particle formation in China. *Atmospheric Chemistry and Physics* **19**(1): 115–138. DOI: http://dx.doi.org/10.5194/acp-19-115-2019.

Clarke, AD. 1993. Atmospheric nuclei in the Pacific midtroposphere: Their nature, concentration, and evolution. *Journal of Geophysical Research: Atmospheres* **98**(D11): 20633. DOI: http://dx.doi.org/10.1029/93JD00797.

Crawford, JH, **Ahn, J-Y**, **Al-Saadi, J**, **Chang, L**, **Emmons, LK**, **Kim, J**, **Lee, G**, **Park, J-H**, **Park, RJ**, **Woo, JH**, **Song, C-K**, **Hong, J-H**, **Hong, Y-D**, **Lefer, BL**, **Lee, M**, **Lee, T**, **Kim, S**, **Min, K-E**, **Yum, SS**, **Shin, HJ**, **Kim, Y-W**, **Choi, J-S**, **Park, J-S**, **Szykman, JJ**, **Long, RW**, **Jordan, CE**, **Simpson, IJ**, **Fried, A**, **Dibb, JE**, **Cho, SY**, **Kim, YP.** 2021. The Korea–United States Air Quality (KORUS-AQ) field study. *Elementa: Science of the Anthropocene* **9**(1): 00163. DOI: http://dx.doi.org/10.1525/ELEMENTA.2020.00163.

Dall'Osto, M, **Beddows, DCS**, **Asmi, A**, **Poulain, L**, **Hao, L**, **Freney, E**, **Allan, JD**, **Canagaratna, M**, **Crippa, M**, **Bianchi, F**, **de Leeuw, G**, **Eriksson, A**, **Swietlicki, E**, **Hansson, HC**, **Henzing, JS**, **Granier, C**, **Zemankova, K**, **Laj, P**, **Onasch, T**, **Prevot, A**, **Putaud, JP**, **Sellegri, K**, **Vidal, M**, **Virtanen, A**, **Simo, R**, **Worsnop, D**, **O'Dowd, C**, **Kulmala, M**, **Harrison, RM**. 2018. Novel insights on new particle formation derived from a pan-European observing system. *Scientific Reports* **8**(1): 1482. DOI: http://dx.doi.org/10.1038/s41598-017-17343-9.

Ding, AJ, **Huang, X**, **Nie, W**, **Sun, JN**, **Kerminen, V-M**, **Petäjä, T**, **Su, H**, **Cheng, YF**, **Yang, X -Q**, **Wang, MH**, **Chi, XG**, **Wang, JP**, **Virkkula, A**, **Guo, WD**, **Yuan, J**, **Wang, SY**, **Zhang, RJ**, **Wu, YF**, **Song, Y**, **Zhu, T**, **Zilitinkevich, S**, **Kulmala, M**, **Fu, CB.** 2016. Enhanced haze pollution by black carbon in megacities in China. *Geophysical Research Letters* **43**(6): 2873–2879. DOI: http://dx.doi.org/10.1002/2016GL067745.

Elser, M, **Huang, R-J**, **Wolf, R**, **Slowik, JG**, **Wang, Q**, **Canonaco, F**, **Li, G**, **Bozzetti, C**, **Daellenbach, KR**, **Huang, Y**, **Zhang, R**, **Li, Z**, **Cao, J**, **Baltensperger, U**, **Haddad, I-E**, **Prévôt, ASH**. 2016. New insights into $PM_{2.5}$ chemical composition and sources in two major cities in China during extreme haze events using aerosol mass spectrometry. *Atmospheric Chemistry and Physics* **16**(5): 3207–3225. DOI: http://dx.doi.org/10.5194/acp-16-3207-2016.

Engelhart, GJ, **Hildebrandt, L**, **Kostenidou, E**, **Mihalopoulos, N**, **Donahue, NM**, **Pandis, SN.** 2011. Water content of aged aerosol. *Atmospheric Chemistry and Physics* **11**(3): 911–920. DOI: http://dx.doi.org/10.5194/ACP-11-911-2011.

Fan, H, **Zhao, C**, **Yang, Y.** 2020. A comprehensive analysis of the spatio-temporal variation of urban air pollution in China during 2014–2018. *Atmospheric Environment* **220**: 117066. DOI: http://dx.doi.org/10.1016/J.ATMOSENV.2019.117066.

Fountoukis, C, **Nenes, A.** 2007. ISORROPIA II: A computationally efficient thermodynamic equilibrium model for K^+-Ca^{2+}-Mg^{2+}-NH_4^+-Na^+-SO_4^{2-}-NO_3^--Cl^--H_2O aerosols. *Atmospheric Chemistry and Physics* **7**(17): 4639–4659. DOI: http://dx.doi.org/10.5194/acp-7-4639-2007.

Gao, RS, **Schwarz, JP**, **Kelly, KK**, **Fahey, DW**, **Watts, LA**, **Thompson, TL**, **Spackman, JR**, **Slowik, JG**, **Cross, ES**, **Han, J-H**, **Davidovits, P**, **Onasch, TB**, **Worsnop, DR**. 2007. A novel method for estimating light-scattering properties of soot aerosols using a modified single-particle soot photometer. *Aerosol Science and Technology* **41**(2): 125–135. DOI: http://dx.doi.org/10.1080/02786820601118398.

Guo, S, **Hu, M**, **Zamora, ML**, **Peng, J**, **Shang, D**, **Zheng, J**, **Du, Z**, **Wu, Z**, **Shao, M**, **Zeng, L**, **Molina, MJ**, **Zhang, R**. 2014. Elucidating severe urban haze formation in China. *Proceedings of the National Academy of Sciences of the United States of America* **111**(49): 17373–17378. DOI: http://dx.doi.org/10.1073/pnas.1419604111.

Hao, L, **Garmash, O**, **Ehn, M**, **Miettinen, P**, **Massoli, P**, **Mikkonen, S**, **Jokinen, T**, **Roldin, P**, **Aalto, P**, **Yli-Juuti, T**, **Joutsensaari, J**, **Petäjä, T**, **Kulmala, M**, **Lehtinen, KEJ**, **Worsnop, DR**, **Virtanen, A**. 2018. Combined effects of boundary layer dynamics and atmospheric chemistry on aerosol composition during new particle formation periods. *Atmospheric Chemistry and Physics* **18**(23): 17705–17716. DOI: http://dx.doi.org/10.5194/acp-18-17705-2018.

Hirsikko, A, **Nieminen, T**, **Gagné, S**, **Lehtipalo, K**, **Manninen, HE**, **Ehn, M**, **Hõrrak, U**, **Kerminen, V-M**, **Laakso, L**, **McMurry, PH**, **Mirme, A**, **Mirme, S**, **Petäjä, T**, **Tammet, H**, **Vakkari, V**, **Vana, M**, **Kulmala, M**. 2011. Atmospheric ions and nucleation: A review of observations. *Atmospheric Chemistry and Physics* **11**(2): 767–798. DOI: http://dx.doi.org/10.5194/acp-11-767-2011.

Hodas, N, **Sullivan, AP**, **Skog, K**, **Keutsch, FN**, **Collett, JL**, **Decesari, S**, **Facchini, MC**, **Carlton, AG**, **Laaksonen, A**, **Turpin, BJ**. 2014. Aerosol liquid water driven by anthropogenic nitrate: Implications for lifetimes of water-soluble organic gases and potential for secondary organic aerosol formation. *Environmental Science & Technology* **48**(19): 11127–11136. DOI: https://doi.org/10.1021/es5025096.

Huang, Q, **Cai, X**, **Wang, J**, **Song, Y**, **Zhu, T.** 2018. Climatological study of the boundary-layer air stagnation index for China and its relationship with air pollution. *Atmospheric Chemistry and Physics* **18**(10): 7573–7593. DOI: http://dx.doi.org/10.5194/acp-18-7573-2018.

Huang, R-J, **Zhang, Y**, **Bozzetti, C**, **Ho, K-F**, **Cao, J-J**, **Han, Y**, **Daellenbach, KR**, **Slowik, JG**, **Platt, SM**, **Canonaco, F**, **Zotter, P**, **Wolf, R**, **Pieber, SM**, **Bruns, EA**, **Crippa, M**, **Ciarelli, G**, **Piazzalunga, A**, **Schwikowski, M**, **Abbaszade, G**, **Kreis, JS**, **Zimmermann, R**, **An, Z**, **Szidat, S**, **Baltensperger, U**, **Haddad, IE**, **Prévôt, ASH**. 2014. High secondary aerosol contribution to particulate pollution during haze events in China. *Nature* **514**(7521): 218–222. DOI: http://dx.doi.org/10.1038/nature13774.

Jordan, C, **Crawford, JH**, **Beyersdorf, AJ**, **Eck, TF**, **Halliday, HS**, **Nault, BA**, **Chang, L-S**, **Park, J**, **Park, R**, **Lee, G**, **Kim, H**, **Ahn, J-Y**, **Cho, S**, **Shin, HJ**, **Lee, JH**, **Jung, J**, **Kim, DS**, **Lee, M**, **Lee, T**, **Whitehill, A**, **Szykman, J**, **Schueneman, MK**, **Pedro, C-J**, **Jimenez, JL**, **DiGangi, JP**, **Diskin, GS**, **Anderson, BE**, **Moore, RH**, **Ziemba, LD**, **Fenn, MA**, **Hair, JW**, **Kuehn, RE**, **Holz, RE**, **Chen, G**, **Travis, K**, **Shook, M**, **Peterson, DA**, **Lamb, KD**, **Schwarz, JP**. 2020. Investigation of factors controlling $PM_{2.5}$ variability across the South Korean Peninsula during KORUS-AQ. *Elementa: Science of the Anthropocene* **8**(1): 28. DOI: http://dx.doi.org/10.1525/elementa.424.

Kang, E, **Lee, M**, **Brune, WH**, **Lee, T**, **Park, T**, **Ahn, J**, **Shang, X.** 2018. Photochemical aging of aerosol particles in different air masses arriving at Baengnyeong Island, Korea. *Atmospheric Chemistry and Physics* **18**(9): 6661–6677. DOI: http://dx.doi.org/10.5194/acp-18-6661-2018.

Kerminen, V-M, **Chen, X**, **Vakkari, V**, **Petäjä, T**, **Kulmala, M**, **Bianchi, F.** 2018. Atmospheric new particle formation and growth: Review of field observations. *Environmental Research Letters* **13**(10): 103003. DOI: http://dx.doi.org/10.1088/1748-9326/aadf3c.

Khalizov, AF, **Xue, H**, **Wang, L**, **Zheng, J**, **Zhang, R.** 2009. Enhanced light absorption and scattering by carbon soot aerosol internally mixed with sulfuric acid. *Journal of Physical Chemistry A* **113**(6): 1066–1074. DOI: http://dx.doi.org/10.1021/jp807531n.

Kim, H, **Zhang, Q**, **Heo, J.** 2018. Influence of intense secondary aerosol formation and long-range transport on aerosol chemistry and properties in the Seoul metropolitan area during spring time: Results from KORUS-AQ. *Atmospheric Chemistry and Physics* **18**(10): 7149–7168. DOI: http://dx.doi.org/10.5194/acp-18-7149-2018.

Kim, Y, **Kim, S-W**, **Yoon, S-C**. 2014. Observation of new particle formation and growth under cloudy conditions at Gosan Climate Observatory, Korea. *Meteorology and Atmospheric Physics* **126**(1–2): 81–90. DOI: http://dx.doi.org/10.1007/s00703-014-0336-2.

Kim, Y, **Yoon, S-C**, **Kim, S-W**, **Kim, K-Y**, **Lim, H-C**, **Ryu, J.** 2013. Observation of new particle formation and growth events in Asian continental outflow. *Atmospheric Environment* **64**: 160–168. DOI: http://dx.doi.org/10.1016/J.ATMOSENV.2012.09.057.

Kiselev, A, **Wennrich, C**, **Stratmann, F**, **Wex, H**, **Henning, S**, **Mentel, TF**, **Kiendler-Scharr, A**, **Schneider, J**, **Walter, S**, **Lieberwirth, I.** 2010. Morphological characterization of soot aerosol particles during LACIS Experiment in November (LExNo). *Journal of Geophysical Research: Atmospheres* **115**(D11): D11204. DOI: http://dx.doi.org/10.1029/2009JD012635.

Kulmala, M, **Kerminen, V-M.** 2008. On the formation and growth of atmospheric nanoparticles. *Atmospheric Research* **90**(2–4): 132–150. DOI: http://dx.doi.org/10.1016/J.ATMOSRES.2008.01.005.

Kulmala, M, **Kerminen, V-M**, **Petäjä, T**, **Ding, AJ**, **Wang, L.** 2017. Atmospheric gas-to-particle conversion: Why NPF events are observed in megacities? *Faraday Discussions* **200**(0): 271–288. DOI: http://dx.doi.org/10.1039/C6FD00257A.

Laborde, M, **Crippa, M**, **Tritscher, T**, **Jurányi, Z**, **Decarlo, PF**, **Temime-Roussel, B**, **Marchand, N**, **Eckhardt, S**, **Stohl, A**, **Baltensperger, U**, **Prévôt, ASH**, **Weingartner, E**, **Gysel, M**. 2013. Black carbon physical properties and mixing state in the European megacity Paris. *Atmospheric Chemistry and Physics* **13**(11): 5831–5856. DOI: http://dx.doi.org/10.5194/acp-13-5831-2013.

Laborde, M, **Mertes, P**, **Zieger, P**, **Dommen, J**, **Baltensperger, U**, **Gysel, M.** 2012. Sensitivity of the single particle soot photometer to different black carbon types. *Atmospheric Measurement Techniques* **5**(5): 1031–1043. DOI: http://dx.doi.org/10.5194/amt-5-1031-2012.

Lee, H-J, **Jo, H-Y**, **Kim, S-W**, **Park, M-S**, **Kim, C-H**. 2019. Impacts of atmospheric vertical structures on transboundary aerosol transport from China to South Korea. *Scientific Reports* **9**(1): 13040. DOI: http://dx.doi.org/10.1038/s41598-019-49691-z.

Lee, H-K, **Hwang, I-K**, **Ahn, K-H.** 2014. Development and evaluation of Hy-CPC. *Part Aerosol Research* **10**(3): 93–97.

Lelieveld, J, **Evans, JS**, **Fnais, M**, **Giannadaki, D**, **Pozzer, A.** 2015. The contribution of outdoor air pollution sources to premature mortality on a global scale. *Nature* **525**(7569): 367–371. DOI: http://dx.doi.org/10.1038/nature15371.

Leung, DM, **Tai, APK**, **Mickley, LJ**, **Moch, JM**, **van Donkelaar, A**, **Shen, L**, **Martin, RV.** 2018. Synoptic meteorological modes of variability for fine particulate matter ($PM_{2.5}$) air quality in major metropolitan regions of China. *Atmospheric Chemistry and Physics* **18**(9): 6733–6748. DOI: http://dx.doi.org/10.5194/acp-18-6733-2018.

Li, M, **Wang, L**, **Liu, J**, **Gao, W**, **Song, T**, **Sun, Y**, **Li, L**, **Li, X**, **Yonghong, W**, **Liu, L**, **Daellenbach, KR**, **Paasonen, PJ**, **Kerminen, V-M**, **Kulmala, M**, **Wang, Y.** 2020. Exploring the regional pollution characteristics and meteorological formation mechanism of $PM_{2.5}$ in North China during 2013–2017. *Environment International* **134**: 105283. DOI: http://dx.doi.org/10.1016/J.ENVINT.2019.105283.

Liang, X, **Li, S**, **Zhang, S**, **Huang, H**, **Chen, SX.** 2016. $PM_{2.5}$ data reliability, consistency, and air quality assessment in five Chinese cities. *Journal of Geophysical Research: Atmospheres* **121**(17): 10220–10236. DOI: http://dx.doi.org/10.1002/2016JD024877.

Lim, S, **Lee, M**, **Kim, S-W**, **Laj, P**. 2018. Sulfate alters aerosol absorption properties in East Asian outflow. *Scientific Reports* **8**(1): 5172. DOI: http://dx.doi.org/10.1038/s41598-018-23021-1.

Lim, S, **Lee, M**, **Kim, S-W**, **Yoon, S-C**, **Lee, G**, **Lee, YJ**. 2014. Absorption and scattering properties of organic carbon versus sulfate dominant aerosols at Gosan climate observatory in Northeast Asia. *Atmospheric Chemistry and Physics* **14**(15): 7781–7793. DOI: http://dx.doi.org/10.5194/acp-14-7781-2014.

Lim, S, **Lee, M**, **Lee, G**, **Kim, S**, **Yoon, S**, **Kang, K.** 2012. Ionic and carbonaceous compositions of PM_{10}, $PM_{2.5}$ and $PM_{1.0}$ at Gosan ABC superstation and their ratios as source signature. *Atmospheric Chemistry and Physics* **12**(4): 2007–2024. DOI: http://dx.doi.org/10.5194/acp-12-2007-2012.

Lim, S, **Lee, M**, **Savarino, J**, **Laj, P.** 2022. Oxidation pathways and emission sources of atmospheric particulate nitrate in Seoul: Based on δ15 N and Δ17O measurements. *Atmospheric Chemistry and Physics* **22**(8): 5099–5115. DOI: http://dx.doi.org/10.5194/ACP-22-5099-2022.

Liu, D, **Joshi, R**, **Wang, J**, **Yu, C**, **Allan, JD**, **Coe, H**, **Flynn, MJ**, **Xie, C**, **Lee, J**, **Squires, F**, **Kotthaus, S**, **Grimmond, S**, **Ge, X**, **Sun, Y**, **Fu, P.** 2019. Contrasting physical properties of black carbon in urban Beijing between winter and summer. *Atmospheric Chemistry and Physics* **19**(10): 6749–6769. DOI: http://dx.doi.org/10.5194/acp-19-6749-2019.

Liu, Y, **Wu, Z**, **Wang, Y**, **Xiao, Y**, **Gu, F**, **Zheng, J**, **Tan, T**, **Shang, D**, **Wu, Y**, **Zeng, L**, **Hu, M**, **Bateman, AP**, **Martin, ST**. 2017. Submicrometer particles are in the liquid state during heavy haze episodes in the urban atmosphere of Beijing, China. *Environmental Science & Technology Letters* **4**(10): 427–432. DOI: http://dx.doi.org/10.1021/ACS.ESTLETT.7B00352/SUPPL_FILE/EZ7B00352_SI_001.PDF.

Liu, Z, **Gao, W**, **Yu, Y**, **Hu, B**, **Xin, J**, **Sun, Y**, **Wang, L**, **Wang, G**, **Bi, X**, **Zhang, G**, **Xu, H**, **Cong, Z**, **He, J**, **Xu, J**, **Wang, Y.** 2018. Characteristics of $PM_{2.5}$ mass concentrations and chemical species in urban and background areas of China: Emerging results from the CARE-China network. *Atmospheric Chemistry and Physics* **18**(12): 8849–8871. DOI: http://dx.doi.org/10.5194/acp-18-8849-2018.

Moteki, N, **Kondo, Y.** 2010. Dependence of laser-induced incandescence on physical properties of black carbon aerosols: Measurements and theoretical interpretation. *Aerosol Science and Technology* **44**(8): 663–675. DOI: http://dx.doi.org/10.1080/02786826.2010.484450.

National Institute of Environmental Research. 2021. Air pollution monitoring network installation and operation guidelines 2021. Available at https://www.airkorea.or.kr/web/board/3/267/?page=2&pMENU_NO=145. Accessed 22 July 2022.

Nieminen, T, **Kerminen, V-M**, **Petäjä, T**, **Aalto, PP**, **Arshinov, M**, **Asmi, E**, **Baltensperger, U**, **Beddows, DCS**, **Beukes, JP**, **Collins, D**, **Ding, A**, **Harrison, RM**, **Henzing, B**, **Hooda, R**, **Hu, M**, **Hõrrak, U**, **Kivekäs, N**, **Komsaare, K**, **Krejci, R**, **Kristensson, A**, **Laakso, L**, **Laaksonen, L**, **Leaitch, WR**, **Lihavainen, H**, **Mihalopoulos, N**, **Németh, Z**, **Nie, W**, **O'Dowd, C**, **Salma, I**, **Sellegri, K**, **Svenningsson, B**, **Swietlicki, E**, **Tunved, P**, **Ulevicius, V**, **Vakkari, V**, **Vana, M**, **Wiedensohler, A**, **Wu, Z**, **Virtanen, A**, **Kulmala, M**. 2018. Global analysis of continental boundary layer new particle formation based on long-term measurements. *Atmospheric Chemistry and Physics* **18**(19): 14737–14756. DOI: http://dx.doi.org/10.5194/acp-18-14737-2018.

Ning, G, **Wang, S**, **Yim, SHL**, **Li, J**, **Hu, Y**, **Shang, Z**, **Jinyan, W**, **Jiaxin, W**. 2018. Impact of low-pressure systems on winter heavy air pollution in the northwest Sichuan Basin, China. *Atmospheric Chemistry and Physics* **18**(18): 13601–13615. DOI: http://dx.doi.org/10.5194/acp-18-13601-2018.

Park, D-H, **Kim, S-W**, **Kim, M-H**, **Yeo, H**, **Park, SS**, **Nishizawa, T**, **Shimizu, A**, **Kim, C-H.** 2021. Impacts of local versus long-range transported aerosols on PM_{10} concentrations in Seoul, Korea: An estimate based on 11-year PM_{10} and lidar observations. *Science of the Total Environment* **750**: 141739. DOI: http://dx.doi.org/10.1016/J.SCITOTENV.2020.141739.

Park, SM, **Song, IH**, **Park, JS**, **Oh, J**, **Moon, KJ**, **Shin, HJ**, **Ahn, JY**, **Do, LM**, **Kim, J**, **Lee, G.** 2018. Variation of $PM_{2.5}$ chemical compositions and their contributions to light extinction in Seoul. *Aerosol and Air Quality Research* **18**(9): 2220–2229. DOI: http://dx.doi.org/10.4209/AAQR.2017.10.0369.

Peterson, DA, **Hyer, EJ**, **Han, S-O**, **Crawford, JH**, **Park, RJ**, **Holz, R**, **Kuehn, RE**, **Eloranta, E**, **Knote, C**, **Jordan, CE**, **Lefer, BL**. 2019. Meteorology influencing springtime air quality, pollution transport, and visibility in Korea. *Elementa: Science of the Anthropocene* **7**(1): 57. DOI: https://doi.org/10.1525/elementa.395.

Petzold, A, **Ogren, JA**, **Fiebig, M**, **Laj, P**, **Li, S-M**, **Baltensperger, U**, **Holzer-Popp, T**, **Kinne, S**, **Pappalardo, G**, **Sugimoto, N**, **Wehrli, C**, **Wiedensohler, A**, **Zhang, X-Y**. 2013. Recommendations for reporting "black carbon" measurements. *Atmospheric Chemistry and Physics* **13**(16): 8365–8379. DOI: http://dx.doi.org/10.5194/acp-13-8365-2013.

Pilinis, C, **Seinfeld, JH**, **Grosjean, D**. 1989. Water content of atmospheric aerosols. *Atmospheric Environment* **23**(7): 1601–1606. DOI: http://dx.doi.org/10.1016/0004-6981(89)90419-8.

Quan, J, **Dou, Y**, **Zhao, X**, **Liu, Q**, **Sun, Z**, **Pan, Y**, **Jia, X**, **Cheng, Z**, **Ma, P**, **Su, J**, **Xin, J**, **Liu, Y**. 2020. Regional atmospheric pollutant transport mechanisms over the North China Plain driven by topography and planetary boundary layer processes. *Atmospheric Environment* **221**: 117098. DOI: http://dx.doi.org/10.1016/J.ATMOSENV.2019.117098.

Querol, X, **Alastuey, A**, **Gangoiti, G**, **Perez, N**, **Lee, HK**, **Eun, HR**, **Park, Y**, **Mantilla, E**, **Escudero, M**, **Titos, G**, **Alonso, L**, **Roussel, B-T**, **Marchand, N**, **Moreta, JR**, **Revuelta, MA**, **Salvador, P**, **Artíñano, B**, **dos Santos, SG**, **Anguas, M**, **Notario, A**, **Saiz-Lopez, A**, **Harrison, RM**, **Millán, M**, **Ahn, K-H**. 2018. Phenomenology of summer ozone episodes over the Madrid Metropolitan Area, central Spain. *Atmospheric Chemistry and Physics* **18**(9): 6511–6533. DOI: http://dx.doi.org/10.5194/acp-18-6511-2018.

Querol, X, **Gangoiti, G**, **Mantilla, E**, **Alastuey, A**, **Minguillón, MC**, **Amato, F**, **Reche, C**, **Viana, M**, **Moreno, T**, **Karanasiou, A**, **Rivas, I**, **Pérez, N**, **Ripoll, A**, **Brines, M**, **Ealo, M**, **Pandolfi, M**, **Lee, H-K**, **Eun, H-K**, **Park, Y-H**, **Escudero, M**, **Beddows, D**, **Harrison, RM**, **Bertrand, A**, **Marchand, N**, **Lyasota, A**, **Codina, B**, **Olid, M**, **Udina, M**, **Jiménez-Esteve, B**, **Soler, MR**, **Alonso, L**, **Millán, M**, **Ahn, K-H.** 2017. Phenomenology of high-ozone episodes in NE Spain. *Atmospheric Chemistry and Physics* **17**(4): 2817–2838. DOI: http://dx.doi.org/10.5194/acp-17-2817-2017.

Saxena, P, **Hildemann, LM**, **McMurry, PH**, **Seinfeld, JH.** 1995. Organics alter hygroscopic behavior of atmospheric particles. *Journal of Geophysical Research: Atmospheres* **100**(D9): 18755. DOI: http://dx.doi.org/10.1029/95JD01835.

Schnaiter, M, **Horvath, H**, **Möhler, O**, **Naumann, KH**, **Saathoff, H**, **Schöck, OW.** 2003. UV-VIS-NIR spectral optical properties of soot and soot-containing aerosols. *Journal of Aerosol Science* **34**(10): 1421–1444. DOI: http://dx.doi.org/10.1016/S0021-8502(03)00361-6.

Schwarz, JP, **Gao, RS**, **Fahey, DW**, **Thomson, DS**, **Watts, LA**, **Wilson, JC**, **Reeves, JM**, **Darbeheshti, M**, **Baumgardner, DG**, **Kok, GL**, **Chung, SH**, **Schulz, M**, **Hendricks, J**, **Lauer, A**, **Kärcher, B**, **Slowik, JG**, **Rosenlof, KH**, **Thompson, TL**, **Langford, AO**, **Loewenstein, M**, **Aikin, KC.** 2006. Single-particle measurements of midlatitude black carbon and

light-scattering aerosols from the boundary layer to the lower stratosphere. *Journal of Geophysical Research: Atmospheres* **111**(D16): D16207. DOI: http://dx.doi.org/10.1029/2006JD007076.

Schwarz, JP, **Gao, RS**, **Spackman, JR**, **Watts, LA**, **Thomson, DS**, **Fahey, DW**, **Ryerson, TB**, **Peischl, J**, **Holloway, JS**, **Trainer, M**, **Frost, GJ**, **Baynard, T**, **Lack, DA**, **De Gouw, JA**, **Warneke, C**, **Del Negro, LA**. 2008. Measurement of the mixing state, mass, and optical size of individual black carbon particles in urban and biomass burning emissions. *Geophysical Research Letters* **35**(13): L13810. DOI: http://dx.doi.org/10.1029/2008GL033968.

Seidel, DJ, **Ao, CO**, **Li, K.** 2010. Estimating climatological planetary boundary layer heights from radiosonde observations: Comparison of methods and uncertainty analysis. *Journal of Geophysical Research: Atmospheres* **115**(D16): D16113. DOI: http://dx.doi.org/10.1029/2009JD013680.

Sellegri, K, **Laj, P**, **Marinoni, A**, **Dupuy, R**, **Legrand, M**, **Preunkert, S.** 2003. Contribution of gaseous and particulate species to droplet solute composition at the Puy de Dôme, France. *Atmospheric Chemistry and Physics* **3**(5): 1509–1522. DOI: http://dx.doi.org/10.5194/acp-3-1509-2003.

Shi, C, **Nduka, IC**, **Yang, Y**, **Huang, Y**, **Yao, R**, **Zhang, H**, **He, B**, **Xie, C**, **Wang, Z**, **Yim, SHL.** 2020. Characteristics and meteorological mechanisms of transboundary air pollution in a persistent heavy $PM_{2.5}$ pollution episode in Central-East China. *Atmospheric Environment* **223**: 117239. DOI: http://dx.doi.org/10.1016/J.ATMOSENV.2019.117239.

Shin, HJ, **Park, SM**, **Park, JS**, **Song, IH**, **Hong, YD**. 2016. Chemical characteristics of high PM episodes occurring in spring 2014, Seoul, Korea. *Advances in Meteorology* **2016**. DOI: http://dx.doi.org/10.1155/2016/2424875.

Sihto, SL, **Kulmala, M**, **Kerminen, VM**, **Dal Maso, M**, **Petäjä, T**, **Riipinen, I**, **Korhonen, H**, **Arnold, F**, **Janson, R**, **Boy, M**, **Laaksonen, A**, **Lehtinen, KEJ**. 2006. Atmospheric sulphuric acid and aerosol formation: Implications from atmospheric measurements for nucleation and early growth mechanisms. *Atmospheric Chemistry and Physics* **6**(12): 4079–4091. DOI: http://dx.doi.org/10.5194/ACP-6-4079-2006.

Song, M, **Lee, M**, **Kim, JH**, **Yum, SS**, **Lee, G**, **Kim, K-R.** 2010. New particle formation and growth in relation to vertical mixing and chemical species during ABC-EAREX2005. *Atmospheric Research* **97**(3): 359–370. DOI: http://dx.doi.org/10.1016/J.ATMOSRES.2010.04.013.

Stephens, M, **Turner, N**, **Sandberg, J.** 2003. Particle identification by laser-induced incandescence in a solid-state laser cavity. *Applied Optics* **42**(19): 3726–3736.

Takegawa, N, **Seto, T**, **Moteki, N**, **Koike, M**, **Oshima, N**, **Adachi, K**, **Kita, K**, **Takami, A**, **Kondo, Y.** 2020. Enhanced new particle formation above the marine boundary layer over the Yellow Sea: Potential impacts on cloud condensation nuclei. *Journal of Geophysical Research: Atmospheres* **125**(9): e2019JD031448. DOI: http://dx.doi.org/10.1029/2019JD031448.

Taylor, JW, **Allan, JD**, **Liu, D**, **Flynn, M**, **Weber, R**, **Zhang, X**, **Lefer, BL**, **Grossberg, N**, **Flynn, J**, **Coe, H.** 2015. Assessment of the sensitivity of core/shell parameters derived using the single-particle soot photometer to density and refractive index. *Atmospheric Measurement Techniques* **8**(4): 1701–1718. DOI: http://dx.doi.org/10.5194/amt-8-1701-2015.

Tian, P, **Liu, D**, **Huang, M**, **Liu, Q**, **Zhao, D**, **Ran, L**, **Deng, Z**, **Wu, Y**, **Fu, S**, **Bi, K**, **Gao, Q**, **He, H**, **Xue, H**, **Ding, D.** 2019. The evolution of an aerosol event observed from aircraft in Beijing: An insight into regional pollution transport. *Atmospheric Environment* **206**: 11–20. DOI: http://dx.doi.org/10.1016/J.ATMOSENV.2019.02.005.

Toon, OB, **Pollack, JB**, **Khare, BN.** 1976. The optical constants of several atmospheric aerosol species: Ammonium sulfate, aluminum oxide, and sodium chloride. *Journal of Geophysical Research* **81**(33): 5733–5748. DOI: http://dx.doi.org/10.1029/JC081I033P05733.

Ueda, S, **Nakayama, T**, **Taketani, F**, **Adachi, K**, **Matsuki, A**, **Iwamoto, Y**, **Sadanaga, Y**, **Matsumi, Y**. 2016. Light absorption and morphological properties of soot-containing aerosols observed at an East Asian outflow site, Noto Peninsula, Japan. *Atmospheric Chemistry and Physics* **16**(4): 2525–2541. DOI: http://dx.doi.org/10.5194/acp-16-2525-2016.

Wang, H, **Li, J**, **Peng, Y**, **Zhang, M**, **Che, H**, **Zhang, X.** 2019. The impacts of the meteorology features on $PM_{2.5}$ levels during a severe haze episode in central-east China. *Atmospheric Environment* **197**: 177–189. DOI: http://dx.doi.org/10.1016/J.ATMOSENV.2018.10.001.

Wang, H, **Tan, SC**, **Wang, Y**, **Jiang, C**, **Shi, G-Y**, **Zhang, MX**, **Che, HZ.** 2014a. A multisource observation study of the severe prolonged regional haze episode over eastern China in January 2013. *Atmospheric Environment* **89**: 807–815. DOI: http://dx.doi.org/10.1016/J.ATMOSENV.2014.03.004.

Wang, H, **Xu, J**, **Zhang, M**, **Yang, Y**, **Shen, X**, **Wang, Y**, **Chen, D**, **Guo, J.** 2014b. A study of the meteorological causes of a prolonged and severe haze episode in January 2013 over central-eastern China. *Atmospheric Environment* **98**: 146–157. DOI: http://dx.doi.org/10.1016/J.ATMOSENV.2014.08.053.

Wang, Q, **Huang, R-J**, **Cao, J**, **Tie, X**, **Shen, Z**, **Zhao, S**, **Han, Y**, **Li, G**, **Li, Z**, **Ni, H**, **Zhou, Y**, **Wang, M**, **Chen, Y**, **Su, X.** 2016. Contribution of regional transport to the black carbon aerosol during winter haze period in Beijing. *Atmospheric Environment* **132**: 11–18. DOI: http://dx.doi.org/10.1016/J.ATMOSENV.2016.02.031.

Weber, RJ, **Marti, JJ**, **McMurry, PH**, **Eisele, FL**, **Tanner, DJ**, **Jefferson, A.** 1996. Measured atmospheric new particle formation rates: Implications for nucleation mechanisms. *Chemical Engineering Communications*

151(1): 53–64. DOI: http://dx.doi.org/10.1080/00986449608936541.

Wiedensohler, A, **Cheng, YF**, **Nowak, A**, **Wehner, B**, **Achtert, P**, **Berghof, M**, **Birmili, W**, **Wu, ZJ**, **Hu, M**, **Zhu, T**, **Takegawa, N**, **Kita, K**, **Kondo, Y**, **Lou, SR**, **Hofzumahaus, A**, **Holland, F**, **Wahner, A**, **Gunthe, SS**, **Rose, D**, **Su, H**, **Pöschl, U**. 2009. Rapid aerosol particle growth and increase of cloud condensation nucleus activity by secondary aerosol formation and condensation: A case study for regional air pollution in northeastern China. *Journal of Geophysical Research: Atmospheres* **114**(D2): D00G08. DOI: http://dx.doi.org/10.1029/2008JD010884.

Wu, Z, **Hu, M**, **Liu, S**, **Wehner, B**, **Bauer, S**, **Ssling, AM**, **Wiedensohler, A**, **Petäjä, T**, **Maso, MD**, **Kulmala, M.** 2007. New particle formation in Beijing, China: Statistical analysis of a 1-year data set. *Journal of Geophysical Research: Atmospheres* **112**(D9): D09209. DOI: http://dx.doi.org/10.1029/2006JD007406.

Wu, Z, **Wang, Y**, **Tan, T**, **Zhu, Y**, **Li, M**, **Shang, D**, **Wang, H**, **Lu, K**, **Guo, S**, **Zeng, L**, **Zhang, Y**. 2018. Aerosol liquid water driven by anthropogenic inorganic salts: Implying its key role in haze formation over the North China Plain. *Environmental Science & Technology Letters* **5**(3): 160–166. DOI: http://dx.doi.org/10.1021/acs.estlett.8b00021.

Xue, J, **Griffith, SM**, **Yu, X**, **Lau, AKH**, **Yu, JZ**. 2014. Effect of nitrate and sulfate relative abundance in $PM_{2.5}$ on liquid water content explored through half-hourly observations of inorganic soluble aerosols at a polluted receptor site. *Atmospheric Environment* **99**: 24–31. DOI: https://doi.org/10.1016/j.atmosenv.2014.09.049.

Yang, T, **Sun, Y**, **Zhang, W**, **Wang, Z**, **Liu, X**, **Fu, P**, **Wang, X.** 2017. Evolutionary processes and sources of high-nitrate haze episodes over Beijing, Spring. *International Journal of Environmental Science and Technology* **54**: 142–151. Elsevier. DOI: http://dx.doi.org/10.1016/J.JES.2016.04.024.

Yang, X, **Zhao, C**, **Guo, J**, **Wang, Y.** 2016. Intensification of aerosol pollution associated with its feedback with surface solar radiation and winds in Beijing. *Journal of Geophysical Research: Atmospheres* **121**(8): 4093–4099. DOI: http://dx.doi.org/10.1002/2015JD024645.

Ye, X, **Song, Y**, **Cai, X**, **Zhang, H.** 2016. Study on the synoptic flow patterns and boundary layer process of the severe haze events over the North China Plain in January 2013. *Atmospheric Environment* **124**: 129–145. DOI: http://dx.doi.org/10.1016/J.ATMOSENV.2015.06.011.

Yeo, M-J, **Kim, Y-S**, **Yoo, S-S**, **Jeon, E-M**, **Kim, Y-P.** 2019. Long-term trend of $PM_{2.5}$ concentration in Seoul. *Journal of Korean Society for Atmospheric Environment* **35**(4): 438–450.

Zanatta, M, **Laj, P**, **Gysel, M**, **Baltensperger, U**, **Vratolis, S**, **Eleftheriadis, K**, **Kondo, Y**, **Dubuisson, P**, **Winiarek, V**, **Kazadzis, S**, **Tunved, P**, **Jacobi, H-B**. 2018. Effects of mixing state on optical and radiative properties of black carbon in the European Arctic. *Atmospheric Chemistry and Physics* **18**(19): 14037–14057. DOI: http://dx.doi.org/10.5194/acp-18-14037-2018.

Zhang, H, **Yuan, H**, **Liu, X**, **Yu, J**, **Jiao, Y.** 2018. Impact of synoptic weather patterns on 24 h-average $PM_{2.5}$ concentrations in the North China Plain during 2013–2017. *Science of the Total Environment* **627**: 200–210. DOI: http://dx.doi.org/10.1016/J.SCITOTENV.2018.01.248.

Zhang, Q, **Quan, J**, **Tie, X**, **Li, X**, **Liu, Q**, **Gao, Y**, **Zhao, D.** 2015. Effects of meteorology and secondary particle formation on visibility during heavy haze events in Beijing, China. *Science of the Total Environment* **502**: 578–584. DOI: http://dx.doi.org/10.1016/j.scitotenv.2014.09.079.

Zhang, R, **Khalizov, AF**, **Pagels, J**, **Zhang, D**, **Xue, H**, **McMurry, PH.** 2008. Variability in morphology, hygroscopicity, and optical properties of soot aerosols during atmospheric processing. *Proceedings of the National Academy of Sciences of the United States of America* **105**(30): 10291–10296. DOI: http://dx.doi.org/10.1073/pnas.0804860105.

Zhang, R, **Wooldridge, PJ**, **Abbatt, JPD**, **Molina, MJ.** 1993. Physical chemistry of the sulfuric acid/water binary system at low temperatures: Stratospheric implications. *The Journal of Physical Chemistry A* **97**(28): 7351–7358. DOI: http://dx.doi.org/10.1021/j100130a038.

Zheng, H, **Kong, S**, **Wu, F**, **Cheng, Y**, **Niu, Z**, **Zheng, S**, **Yang, G**, **Yao, L**, **Yan, Q**, **Wu, J**, **Zheng, M**, **Chen, N**, **Xu, K**, **Yan, Y**, **Liu, D**, **Zhao, D**, **Zhao, T**, **Bai, Y**, **Li, S**, **Qi, S**. 2019. Intra-regional transport of black carbon between the south edge of the North China Plain and central China during winter haze episodes. *Atmospheric Chemistry and Physics* **19**(7): 4499–4516. DOI: http://dx.doi.org/10.5194/acp-19-4499-2019.

Zhong, J, **Zhang, X**, **Dong, Y**, **Wang, Y**, **Liu, C**, **Wang, J**, **Zhang, Y**, **Che, H.** 2018. Feedback effects of boundary-layer meteorological factors on cumulative explosive growth of $PM_{2.5}$ during winter heavy pollution episodes in Beijing from 2013 to 2016. *Atmospheric Chemistry and Physics* **18**(1): 247–258. DOI: http://dx.doi.org/10.5194/acp-18-247-2018.

Zhou, Y, **Zhang, H**, **Parikh, HM**, **Chen, EH**, **Rattanavaraha, W**, **Rosen, EP**, **Wang, W**, **Kamens, RM**. 2011. Secondary organic aerosol formation from xylenes and mixtures of toluene and xylenes in an atmospheric urban hydrocarbon mixture: Water and particle seed effects (II). *Atmospheric Environment* **45**(23): 3882–3890. DOI: https://doi.org/10.1016/j.atmosenv.2010.12.048.

How to cite this article: Lim, S, Lee, M, Laj, P, Kim, S-W, Ahn, K-H, Gil, J, Shang, X, Zanatta, M, Kang, K-S. 2022. Regional characteristics of fine aerosol mass increase elucidated from long-term observations and KORUS-AQ campaign at a Northeast Asian background site. *Elementa: Science of the Anthropocene* 10(1). DOI: https://doi.org/10.1525/elementa.2022.00020

Domain Editor-in-Chief: Detlev Helmig, Boulder AIR LLC, Boulder, CO, USA

Associate Editor: Md Firoz Khan, Department of Environmental Science and Management, North South University, Dhaka, Bangladesh

Knowledge Domain: Atmospheric Science

Part of an Elementa Special Feature: Korea-United States Air Quality (KORUS-AQ)

Published: September 30, 2022 **Accepted:** July 13, 2022 **Submitted:** February 2, 2022

ELEMENTA Science of the Anthropocene

Elem Sci Anth is a peer-reviewed open access journal published by University of California Press.

OPEN ACCESS